AFRL-RV-PS-
TR-2017-0146

HIGH CAPACITY CATHODE AND CARBON NANOTUBE-SUPPORTED ANODE FOR ENHANCED ENERGY DENSITY BATTERIES

Brian J. Landi, et al.

Department of Chemical Engineering
Rochester Institute of Technology
160 Lomb Memorial Dr.
Rochester, NY 14604-5603

7 Sep 2017

Final Report

AIR FORCE RESEARCH LABORATORY
Space Vehicles Directorate
3550 Aberdeen Ave SE
AIR FORCE MATERIEL COMMAND
KIRTLAND AIR FORCE BASE, NM 87117-5776

DTIC COPY

NOTICE AND SIGNATURE PAGE

This report is the result of contracted fundamental research which is exempt from public affairs security and policy review in accordance with AFI 61-201, paragraph 2.3.5.1. This report is available to the general public, including foreign nationals. Copies may be obtained from the Defense Technical Information Center (DTIC) (http://www.dtic.mil).

AFRL-RV-PS-TR-2017-0146 HAS BEEN REVIEWED AND IS APPROVED FOR PUBLICATION IN ACCORDANCE WITH ASSIGNED DISTRIBUTION STATEMENT.

//SIGNED//
JESSICA BUCKNER
Program Manager

//SIGNED//
PAUL HAUSGEN, Ph.D.
Technical Advisor, Spacecraft Component Technology

//SIGNED//
JOHN BEAUCHEMIN
Chief Engineer, Spacecraft Technology Division
Space Vehicles Directorate

REPORT DOCUMENTATION PAGE

Form Approved
OMB No. 0704-0188

1. REPORT DATE *(DD-MM-YYYY)*	2. REPORT TYPE	3. DATES COVERED *(From - To)*
07-09-2017	Final Report	31 Jul 2014 – 31 Oct 2017

4. TITLE AND SUBTITLE

High Capacity Cathode and Carbon Nanotube-Supported Anode for Enhanced Energy Density Batteries

5a. CONTRACT NUMBER

5b. GRANT NUMBER

FA9453-14-1-0239

5c. PROGRAM ELEMENT NUMBER

62601F

6. AUTHOR(S)

Brian J. Landi, Matthew Ganter, Christopher Schauerman, Kyle Crompton, Anthony Leggiero, Jason Staub

5d. PROJECT NUMBER

8809

5e. TASK NUMBER

PPM00019600

5f. WORK UNIT NUMBER

EF123409

7. PERFORMING ORGANIZATION NAME(S) AND ADDRESS(ES)

Department of Chemical Engineering
Rochester Institute of Technology
160 Lomb Memorial Dr.
Rochester, NY 14604-5603

8. PERFORMING ORGANIZATION REPORT NUMBER

9. SPONSORING / MONITORING AGENCY NAME(S) AND ADDRESS(ES)

Air Force Research Laboratory
Space Vehicles Directorate
3550 Aberdeen Ave SE
Kirtland AFB, NM 87117-5776

10. SPONSOR/MONITOR'S ACRONYM(S)

AFRL/RVSV

11. SPONSOR/MONITOR'S REPORT NUMBER(S)

AFRL-RV-PS-TR-2017-0146

12. DISTRIBUTION / AVAILABILITY STATEMENT

Approved for public release; distribution is unlimited.

13. SUPPLEMENTARY NOTES

14. ABSTRACT

The work evaluated high capacity cathodes along with high capacity anode materials such as silicon and germanium to reach lithium ion cell energy density of 400 Wh/kg. In addition, an approach of managing the amount of reversible lithium in a cell to prevent the anode potential from increasing to greater than the dissolution potential during near zero volt storage is introduced. Pouch cell demonstrations for mesocarbon microbead anode and lithium cobalt oxide and lithium rich cathodes show stability for days at near zero volts beginning of life; with no measured difference in capacity, rate capability, or cycling. Cathode coating technologies of aluminum phosphate on lithium cobalt oxide improves the discharge stability which can increase energy density. The benefits of carbon nanotube current collectors for anode deposition are evaluated and improved with alumina coatings.

15. SUBJECT TERMS

Energy Density, lithium ion, cathode, anode, zero volt, carbon nanotube, silicon

16. SECURITY CLASSIFICATION OF:			17. LIMITATION OF ABSTRACT	18. NUMBER OF PAGES	19a. NAME OF RESPONSIBLE PERSON
a. REPORT	b. ABSTRACT	c. THIS PAGE			Jessica Buckner
Unclassified	Unclassified	Unclassified	Unlimited	80	19b. TELEPHONE NUMBER *(include area code)*

--- This Page Intentionally Left Blank ---

TABLE OF CONTENTS

LIST OF FIGURES

LIST OF TABLES

ACKNOWLEDGEMENT

This material is based on research sponsored by Air Force Research Laboratory (AFRL) under agreement number FA9453-14-1-0239. The U.S. Government is authorized to reproduce and distribute reprints for Governmental purposes notwithstanding any copyright notation thereon.

DISCLAIMER

The views and conclusions contained herein are those of the authors and should not be interpreted as necessarily representing the official policies or endorsements, either expressed or implied, of the Air Force Research Laboratory or the U.S. Government.

This Page Intentionally Left Blank

1 SUMMARY

Reaching 400 Wh/kg at the cell level could lead to a significant increase in electrification of transportation and the grid, and lower overall cost through the use of a lower number of cells. This incresase is ~2x the energy density of typical lithium ion cells and enables twice the run time or a reduction of cell mass by 50%. This work investigated a variety of materials and engineering techniques that could lead to a commercially viable 400 Wh/kg cell.

Synthesis of lithium rich cathode materials that had published capacites near 300 mAh/g were followed, but it was found that the material was unable to be replicated following multiple paper's procedures. Successful work was generated with charging commercial $LiCoO_2$ to higher voltages where stablitly was enabled throught $AlPO_4$ coatings. The ability to charge to higher voltages increases both capacity and average voltages leading to much higher energy densities exceeding even the lithium rich materials at a 4.6V charge voltage.

These higher voltage cathodes or commercially available lithium rich materials could be paired with high capacity anode materials such as Si and Ge to reach 400 Wh/kg. This work looked to advance Si coatings on carbon nanotube (CNT) current collectors based on previous work in the NanoPower Research Labs (NPRL). The use of CNT current collectors has a significant mass improvement over traditional copper, and allowed a flexible "nano-net" for expansion of the the Si with lithium. Si was successfully coated on CNT current collectors. However, loadings above 2 mAh/cm^2 leads to cracking and likely reduced cycling performance. These materials still hold promise and with further modifications of the process could lead to 400 Wh/kg at higher loadings.

Reaching high levels of energy per mass also leads to potential saftey concerns. There are inherent safety risks associated with inactive lithium ion batteries leading to greater restrictions and regulations on shipping and storage. Maintaining all cells of a lithium ion battery at near zero voltage with an applied fixed load is one promising approach which can lessen (and potentially eliminate) the risk of a lithium ion battery entering thermal runaway when in an inactive state. However, in a conventional lithium ion cell, a near zero cell voltage can be damaging if the anode electrochemical potential increases to greater than the potential where dissolution of the standard copper current collector occurs (i.e. ~3.1 V vs. Li/Li^+ at room temperature). Past approaches to yield lithium ion cells that are resilient to a near zero volt state of charge involve use of secondary active materials or alternative current collectors which have anticipated tradeoffs in terms of cell performance and cost.

In the present work an approach of managing the amount of reversible lithium in a cells to prevent the anode potential from increasing to greater than ~3.1 V vs. Li/Li^+ during near zero volt storage is introduced. Anode pre-lithiation was used in $LiCoO_2$/mesocarbon microbeads (MCMB) pouch cells to appropriately manage the amount of reversible lithium so that there is excess reversible lithium compared to the cathodes intercalation capacity (Reversible lithium excess cell or RLE cell). RLE $LiCoO_2$/MCMB cells maintained 99% of their original capacity after three, 3-day and three, 7-day storage periods at near zero volts under fixed load. A $LiCoO_2$/MCMB pouch cell fabricated with a pre-lithiated anode also maintained its original discharge performance after three, 3-day storage periods under fixed load at 45°C. The strong

recharge performance after near zero volt storage is attributed to the anode potential remaining below the copper dissolution potential during near zero volt storage as informed by reference electrode measurements. Pulse discharge measurements were performed and show that double layer capacitance likely plays a major role in determining the behavior of electrode potentials during near zero volt storage. To further the viability of the anode pre-lithiation method in $LiCoO_2$/MCMB cells, stabilization coatings on the cathode materials are being investigated to increase the tolerance of the cathode to the low potentials it experiences during near zero volt storage of an RLE lithium ion cell. Results show that an $AlPO_4$ coating prevents cation exhange in the cathode crystal structure and substantially increases the cathode's resilience to low electrochemical potentials. Investigations into applying anode pre-lithiation to cells utilizing $LiNiCoAlO_2$ (NCA) cathodes have also been initiated and found to maintain the anode potential below the copper dissolution potential during near zero volt storage. RLE NCA/MCMB cells showed strong recharge performance and improved rate capability retention over a conventional NCA/MCMB cell after ten, 3-day near zero volt storage periods. The near zero volt storage tolerance of lithium ion cells utilizing an advanced, high energy density lithium rich cathode material ($0.49Li_2MnO_3 \cdot 0.51LiNi_{0.37}Co_{0.24}Mn_{0.39}O_2$ or HE5050) has also been studied and found to be high at room temperature without the need for anode pre-lithiation. HE5050/MCMB cells maintaining 100% of their discharge capacity after five, 3-day and five, 7-day near zero volt storage periods. The high first cycle loss and lower intercalation potential of the HE5050 cathode lead to the anode potential remaining <2.8 V vs. Li/Li^+ during near zero volt storage and as such, no copper dissolution is expected to be occurring. Finally, CNT papers have been shown to be stable up to high potentials vs. Li/Li^+, and thus using them as an anode current collector in place of standard copper can generate lithium ion cells that can tolerate near zero volt storage. However, CNT papers suffer from significant irreversible loss due to their high surface area. An Al_2O_3 coating deposited by atomic layer deposition is invesitgated for its effect in reducing the irreversible losses of a CNT paper and found to reduce irreversible loss by 55% over 50 cycles and still serve as an effective current collector for a graphitic anode composite.

2 INTRODUCTION

There is currently a critical need for improved energy storage devices to support the advancement of space and terrestrial power systems. Lithium ion batteries have emerged as the premier technology due to its increased energy density over other rechargeable chemistries and offer many benefits with improved materials [1-18]. Significant improvements in energy and power density have allowed production of partial or full electric vehicles to greatly increase over the past decade [1]. However, in recent years the lithium ion performance has begun to level off with incremental engineering advancements reaching a commercial cell performance plateau of ~200 Wh/kg. Further gain in lithium ion battery energy density can directly benefit space applications, as well as, terrestrial applications like electric vehicles, grid storage, and portable electronics. Pathways to double the energy density of state-of-the-art (SOA) lithium ion batteries to a goal of 400 Wh/kg, while demonstrating good rate capability, will require improvement in the capacity and performance of both the cathode and anode. The anode has shown tremendous promise recently with nanostructured materials and CNT-enhanced free-standing electrodes [2-4], but the cathode is limited by lower capacities and the typical areal loading of active materials. The cathode capacity needs to be improved along with alternative approaches to electrode design through the use of nanostructured materials in the composite. Thus, it would be a transformational development to develop a cathode system which combines a high capacity active material (e.g. $x\mathrm{Li_2MnO_3}$-$(1\text{-}x)\mathrm{LiMn_{xx}Ni_{xx}Co_{xx}O_2}$ due to the high capacity potential: > 200 mAh/g) with CNT additives that can increase composite loading and offer improved safety due to being high thermal conductivity additives [5].

In order to realize 400 Wh/kg in a full battery, each electrode must be engineered to maximize capacity while minimizing inactive mass. A high capacity cathode has to be paired with an advanced anode design. Therefore, the cathode composite areal loading will be increased to enable matching with higher capacity active anode materials (e.g. Si, Ge). Previous work has demonstrated that CNT conductive additives are necessary to maintain composite integrity and conductivity at the higher loadings. Therefore, CNT additive amount and total cathode composite loading will be optimized to maintain rate capability and cycling. One of the major detriments to cell energy density is the heavy inactive copper current collector currently used in conventional anode designs. By replacing the Cu current collector with a lightweight CNT paper, a 20% increase in cell energy density can be realized. Commercial MCMB materials, as well as high capacity Si and Ge materials, will be coated or deposited onto CNT current collectors and paired with the aforementioned cathode to increase energy density towards the 400 Wh/kg goal.

Another disadvantage of Cu current collectors is the oxidation potential versus lithium which causes failure of the anode under deep discharge conditions (<0.5V) [6-11]. The ability to discharge to a near zero volt state of charge for long periods of storage time offers a number of significant advantages for terrestrial and space applications that are of interest to AFRL. Batteries can be stored for long periods with little maintenance and are then able to work at peak capacity levels. This is beneficial for space launch situations where infrequent maintenance or trickle charging is often a concern. Also, long term and low maintenance storage of batteries can lead to the ability to stockpile cells and reduce cost for terrestrial use.

Finally, the high energy density cells were evaluated based upon cycling performance for both space and terrestrial applications. Specific to Air Force, there is expressed interest in cycling performance under Geostationary (GEO) and medium/high earth orbit (MEO/HEO) conditions, which are also used for commercial global positioning system (GPS) systems. This work will pair high capacity cathodes with the advanced anodes and cycle under GEO conditions which have slower charge rate and a deeper discharge than LEO.

3 METHODS, ASSUMPTIONS, AND PROCEDURES

3.1 Lithium ion battery standard fabrication

Lithium ion battery electrodes are prepared via a slurry coating process to coat the active material composite onto a current collector (typically a metal foil). In short, the components of the electrode composite, including the active material, a conductive additive (usually graphite, amorphous carbon, or other carbon allotrope) and binder material (often polyvinylidene fluoride (PVDF)) are mixed into an organic solvent (most commonly N-methyl pyrrolidone (NMP)) to form a slurry. The slurry is then cast onto a current collector (typically aluminum foil for the cathode and copper foil for the anode) by a doctor blade on one or both sides of the foil. The composite is dried in a vacuum oven, then calendared to compress the composite. Electrodes are then punched from the prepared composites and assembled into cells.

The active materials used in the cathode and anode have a defined specific capacity, which is the amount of lithium they can reversibly intercalate/de-intercalate per gram of the material over a particular potential range. $LiCoO_2$ cathode material for instance has a specific capacity of ~140 mAh/g when cycled between the potentials 3.0-4.2 V vs. Li/Li^+. Graphite anode material has a practical specific capacity of 300-330 mAh/g when cycled between 0.005-1.5 V vs. Li/Li^+. Depending on the mass loading of the composite (mg/cm^2), electrodes will have a corresponding areal capacity (mAh/cm^2).

Cells are assembled in an argon glove box maintained at <1 ppm O_2 and <1 ppm water or in a dry room to minimize water contamination of the cell. An electrolyte solution consisting of a lithium salt dissolved in an organic solvent or combination of organic solvents (1.2M $LiPF_6$ in 3:7 volume ratio of ethylene carbon (EC) and ethyl methyl carbonate (EMC) is a common formulation) is injected prior to sealing the laminate. An Arbin BT2000 cycler is used for cycling the cells. For cells with a reference electrode, the cell voltage and the electrochemical potential of each electrode with respect to the reference are measured independently throughout cycling. For testing, pouch cells are compressed between restraint plates as depicted in Figure 1b. A rubber slab was placed on one side of the cell in the restraint plates to ensure even pressure and comply with expansion and contraction of the cell upon cycling. Testing is done at room temperature unless otherwise specified.

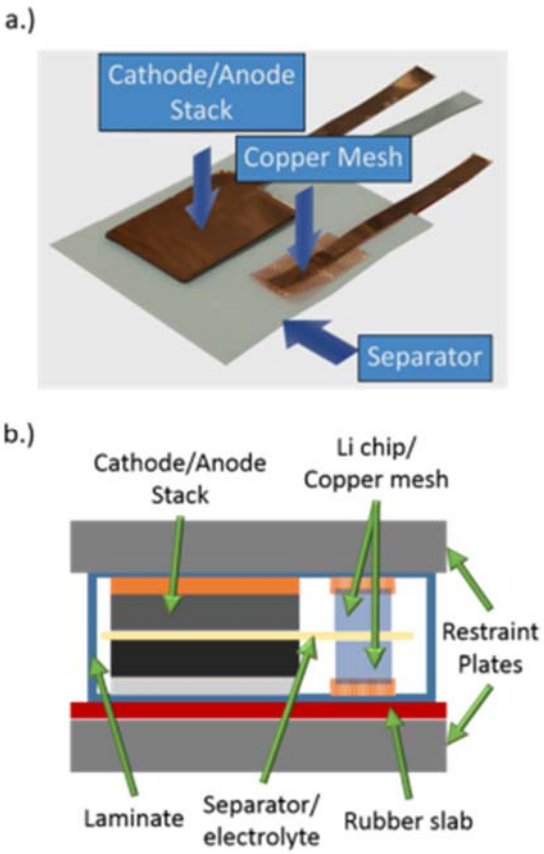

Figure 1. (a) Image of the arrangement of the separator, cathode, anode and reference Li electrode in the pouch cell, (b) Cross sectional schematic of assembled pouch cells placed between restraint plates for testing.

Note: Figure 1 reproduced from reference 17

3.2 Reference electrodes in pouch cells

A lithium metal reference electrode is used to measure the individual electrochemical potential of the cathode and anode during cycling. The design used in the present work, as shown in Figure 1a and b, places the reference electrode on either side of the cathode/anode stack in the pouch cell, which is a setup that has been used successfully by others. As shown in Figure 1b, the reference electrode used in this study consists of a lithium metal foil pressed onto copper mesh that is ultrasonically welded to a copper tab. The lithium-Cu mesh is placed on both sides of the separator to ensure good contact with the electrolyte soaked separator when the cell is compressed between restraint plates during testing, as depicted in Figure 1b.

3.3 Arbin Cyclers and cycling protocols

Arbin cyclers are capable of constant current cycling by application of a varying potential according to equation 1, often done in terms of C-rate (1C = complete charge/discharge in 1

hour, 2C = complete charge/discharge in 30 minutes, etc.). The cyclers can also perform constant voltage by applying a varying current according to equation 1. The cyclers can also apply a fixed load, such as would be accomplished by an applied resistor, by maintaining R constant according to equation 1.

$$V = IR \tag{1}$$

The Arbin cyclers also have auxiliary voltage measurements, which can be used to individually measure the voltage between any chosen electrodes. In the case of a cell with a reference electrode, the potential difference between all three electrodes can be measured independently. The voltage is measured by applying a high impedance (about 10 GOhm) between the electrode and measuring the resulting current flow. The magnitude of the current is <1 nA, so the resulting perturbation of the electrochemical system is negligible.

3.4 Materials Analysis Techniques

Several materials analysis techniques are available for pre- and post-processing and well as pre-cycling and post-mortem. The techniques include:

- **SEM** (scanning electron microscopy) for 2D visualization of micro, meso and nanoscale features
- **XRD** (x-ray diffraction) for examining the crystal structure of cathode and anode active materials to monitor changes or index crystal structure
- **Raman Spectroscopy** for analyzing phonon modes of materials
- **TGA** (thermogravimetric analysis) for analyzing decomposition temperature of materials

4 HIGH CAPACITY CATHODES

4.1 Introduction – Cathodes

The majority of research to improve energy density has focused on increasing the cathode active materials capacity and/or voltage [12-15]. However, the state-of-the-art commercial cathode capacity is still only between 180-200 mAh/g which is lower than the standard anode which has a capacity around 300-330 mAh/g. Cathode vs. anode specific capacities are shown in Figure 2 [16]. Therefore, in order to capacity match the electrode, a higher cathode capacity and/or loading is needed which lowers the battery energy density. Recently, a higher capacity lithium rich cathode material which can reach 250-300 mAh/g was discovered that can better match high capacity anodes. However, higher loadings may still be necessary to match higher capacity Si and Ge anode materials. At higher loadings, a percolation network is more difficult to form, and a new additive may be needed to achieve sufficient performance.

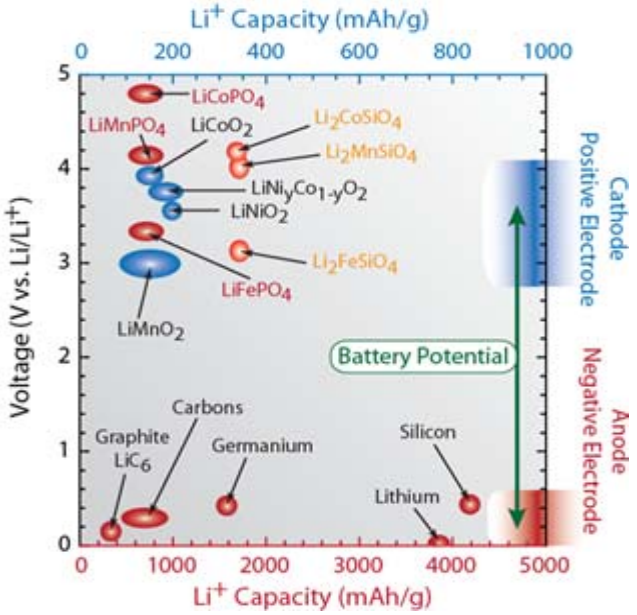

Figure 2. Potential (V) vs. Specific Capacity (mAh/g) of Current Cathode and Anode Active Materials.

Note: Figure 2 reproduced from reference 16

Lithium rich cathode materials with high capacities of 250-300 mAh/g where only recently discovered and are scarcely available commercially. Therefore, the lithium rich materials were synthesized in house to obtain the high capacity material following the procedure published by Argonne National Laboratory, and investigate if any improvement could be made [12]. Rochester Institute of Technology (RIT) also investigated an alternative high capacity layered lithium-rich metal oxide cathode, which was reported to be a hollow $0.3Li_2MnO_3 \bullet 0.7LiNi_{0.5}Mn_{0.5}O_2$ microsphere product with reversible capacities up to 295 mAh/g [13]. The data that was reported showed stable cycling for 100+ cycles, as well as good rate performance up to 2-5C at room temperature. Cycling performance was also shown to be stable at 55C, with a small reduction in

capacity reduction. These increases in cathode capacity would lead to immediate increases in possible lithium ion cell energy densities.

4.2 Methods – Cathode Synthesis

A summary of all the cathode synthesis methods that were pursued are shown in Table 1 below based on references [13-15]. The chemicals used were obtained from Sigma Aldrich. The materials were characterized through XRD, SEM, and TGA analysis, and tested electrochemically using an Arbin BT-2000 cycler.

Table 1. Microsphere Lithium Rich Cathode Publications and Methods [13-15]

He *et. al.* Nano Research, 2014	Jiang *et. al.* Phys. Chem. chem. Phys 2013	Fei *et. al.* Advanced Materials , 2008
Dissolve $MnSO_4$•H2O and NH4CO3 in Ethanol-H20 solution at a **1Mn:1CO_3** molar ratio	Dissolve $MnSO_4$•H2O and NH_4HCO3 in Ethanol-H20 solution at a **1Mn:10CO_3** molar ratio	Dissolve $MnSO_4$•H2O and NH_4HCO3 in Ethanol-H20 solution at a **1Mn:10CO_3** molar ratio
Filter with **water rinses** to obtain $MnCO_3$ Powder	Filter with **water rinses** to obtain $MnCO_3$ Powder	Filter with **alternating water and ethanol rinses** to obtain $MnCO_3$ powder
Oxidize $MnCO_3$ at a heating rate of 1°C/min up to 400°C and hold for 5 hours to get MnO_2	**Oxidize** $MnCO_3$ at a heating rate of 1°C/min up to 400°C and hold for 5 hours to get tetragonal MnO_2	**Chemically oxidize** $MnCO_3$ to MnO_2 with $KMnO_4$. Rinse with HCl to remove remaining reactants.
Disperse MnO_2, LiOH•H_20, $Ni(NO_3)_2$•$6H_20$, and **Co$(NO_3)_2$•6H_20** in **acetone** and slowly evaporate at 50°C	Disperse MnO_2, LiOH•H_20, and $Ni(NO_3)_2$•$6H_20$ in **ethanol** and slowly evaporate at 50°C	
Rinse final product with DI H_20 and sinter at 800°C for 15 hours	**Mortar and pestle final product** and sinter at 800°C for 15 hours	

4.3 Results and Discussion – Cathodes

4.3.1 RIT Lithium Rich Synthesis

The Jiang et al. procedure [13] was initially pursued with the 1 Mn:10 CO_3 molar ratio in reaction of $MnSO_4$ and NH_4CO_3. The MnO_2 microspheres that were created after the reaction and oxidation with ramp to 450°C and hold for 5 hours are shown in Figure 3.

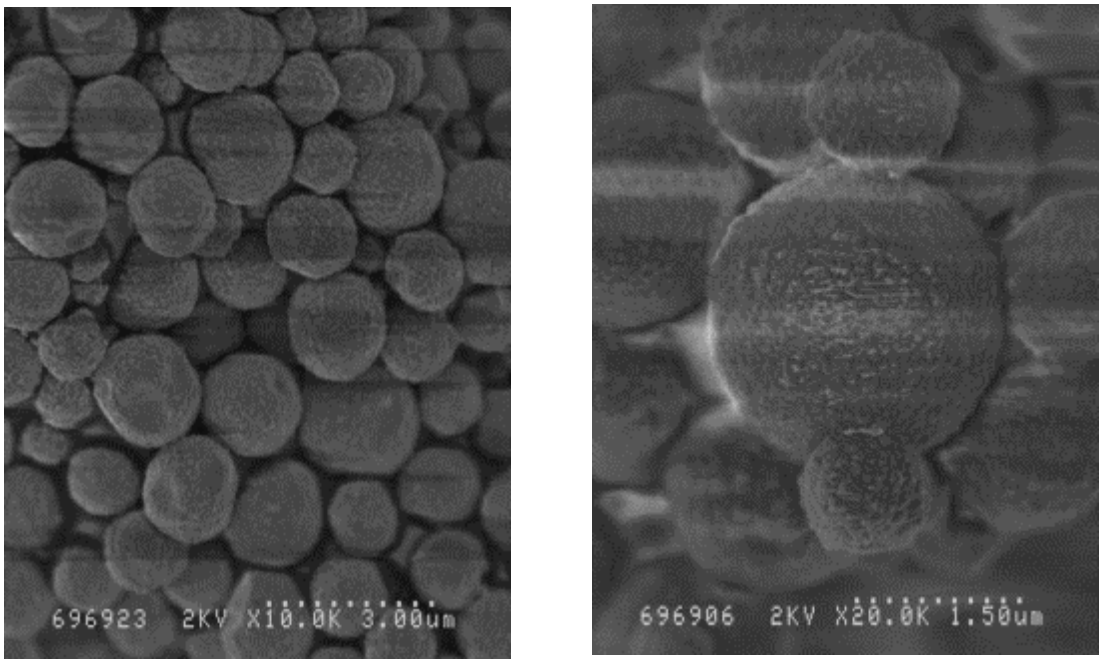

Figure 3. SEM images of synthesized MnO_2 microspheres

The final lithium rich cathode was synthesized by adjusting the moles of lithium hydroxide and nickel nitrate in combination with the MnO_2 microspheres to produce the desired product. The materials were dispersed in ethanol which was slowly evaporated at 50°C. The solid powder was then mortar and pestle before sintering at 800°C for 15 hours. The resulting material was characterized through XRD and SEM analysis which are shown in Figure 4 below. The XRD results match the published values by Jiang et al. However, during the sintering process the spherical shape of the particles was lost as demonstrated by the SEM image. The final product was difficult to image due to low conductivity of the material.

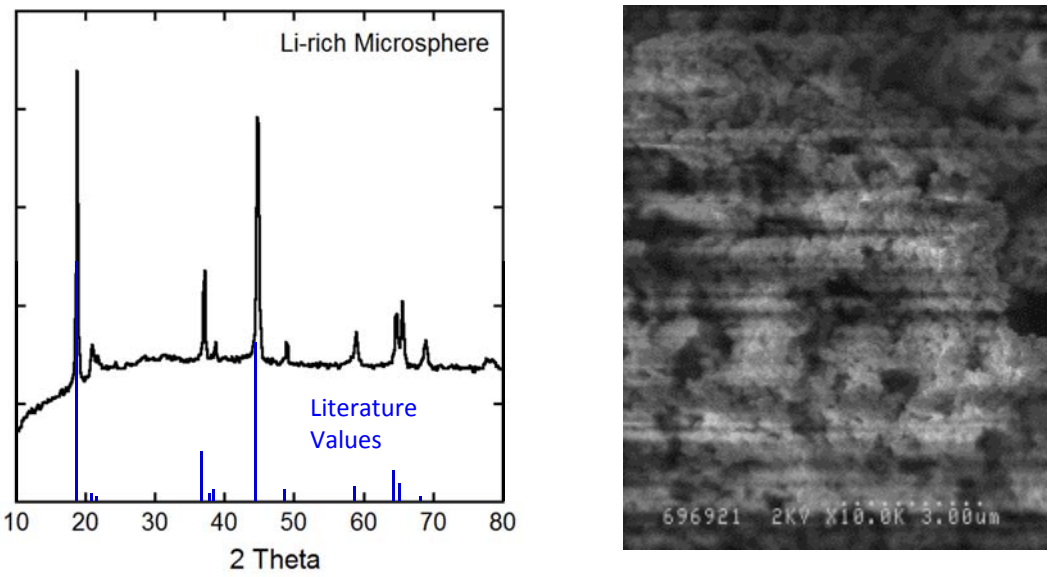

Figure 4. XRD and SEM of Lithium rich microsphere synthesis

The electrochemical performance of the synthesized material was testing in a standard cathode composite at 5 and 10 mAh/g constant current charge-discharge. The voltage profiles are demonstrated in Figure 5 below. The reversible capacity reaches 181 mAh/g at the lower charge/discharge rate. This number is in line with current commercial cathode materials but well below the 300 mAh/g described in the paper.

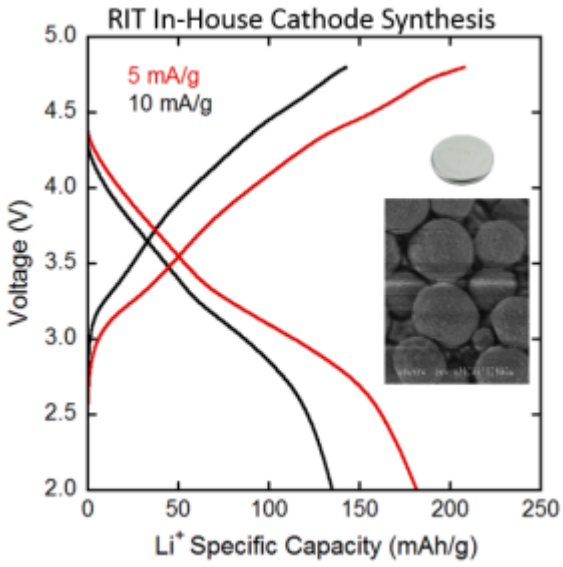

Figure 5. Voltage (V) vs. specific capacity (mAh/g) for Lithium rich cathode synthesized [13]

Following the lower capacity of the Jiang et al. procedure, the He et al. procedure [14] was following to compare synthesis methods. The synthesis process is similar, but has some slight modifications that could result in a different material. The first change is the ratio of molar ratio of Mn:CO_3 which changes form 10:1 to 1:1 following He et al. This ratio change results in microcubes instead of microspheres as evident by the SEM images in Figure 6.

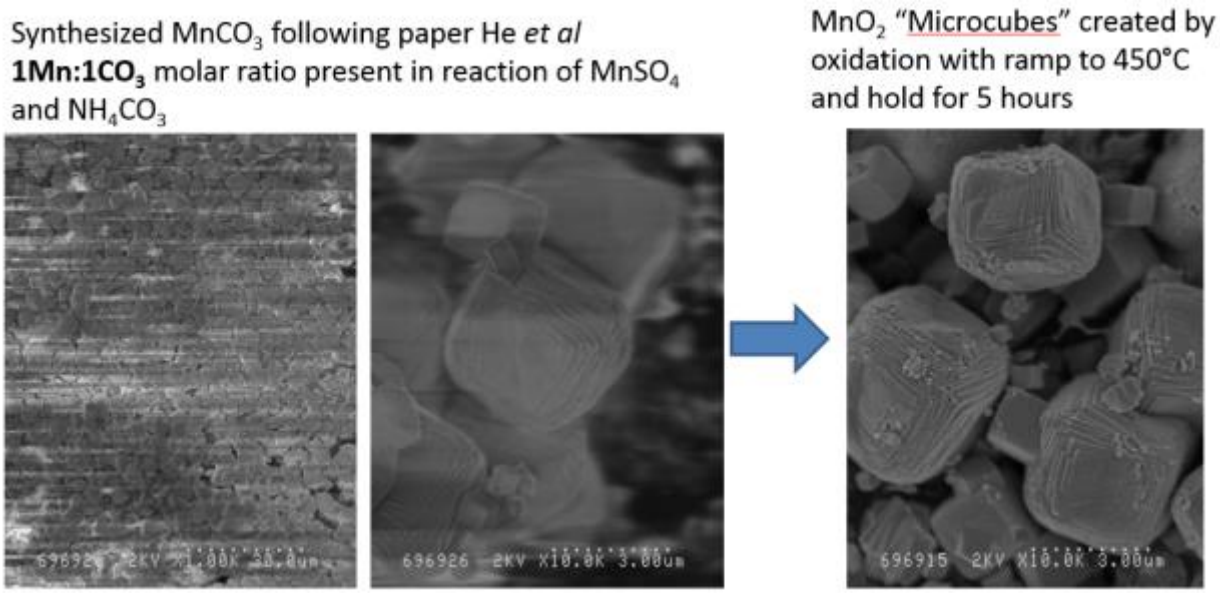

Figure 6. SEM images of MnO_2 microcubes before and after thermal oxidation

The MnO_2 microcubes were mixed and sintered with the lithium and nickel precursors similar to the Jiang et al. paper. The resulting SEM image of the material is demonstrated in the inset in Figure 7 below. The material has a porous structure similar to the paper but in the cube shape of the precursor. However, the electrochemical results were lower than the Jiang et al. paper with an initial capacity of 119 mAh/g which increased to 167 mAh/g after 5 cycles.

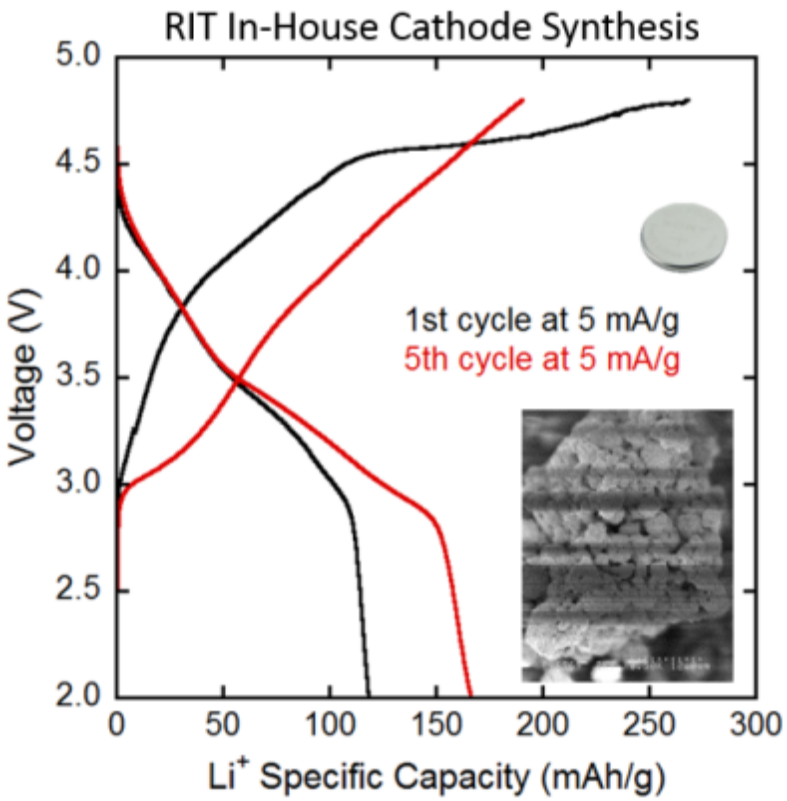

Figure 7. Electrochemical performance at 5 mA/g constant current charge-discharge for lithium rich material synthesized [14]

A final attempt was made to synthesize the microsphere material which would perform well electrochemically by following the Jiang et al. procedure to synthesize the microspheres followed by chemical oxidation with $KMnO_4$ procedure published by Fei et al. [15] to ensure hollow MnO_2 microspheres before lithiation. SEM images of the conversion from $MnCO_3$ to hollow MnO_2 microspheres are shown in Figure 8. The images demonstrate a successful conversion and creation of the hollow microspheres.

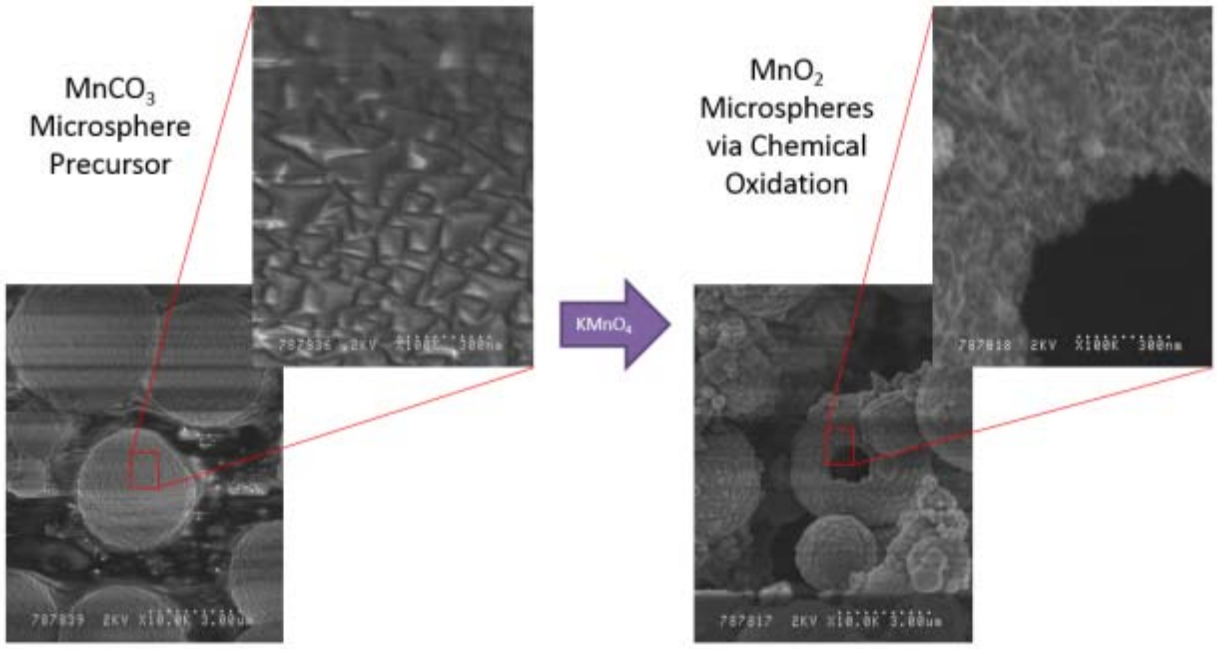

Figure 8. SEM images of $MnCO_3$ conversion to hollow MnO_2 microspheres through chemical oxidation

The lithium rich product was then synthesized from the hollow microspheres following the rest of the Jiang et al. procedure. The XRD in Figure 9 shows good agreement with the published results. The electrochemical performance was again tested using standard cathode formulations and resulted in a capacity of 170 mAh/g which is in line with the other synthesized materials.

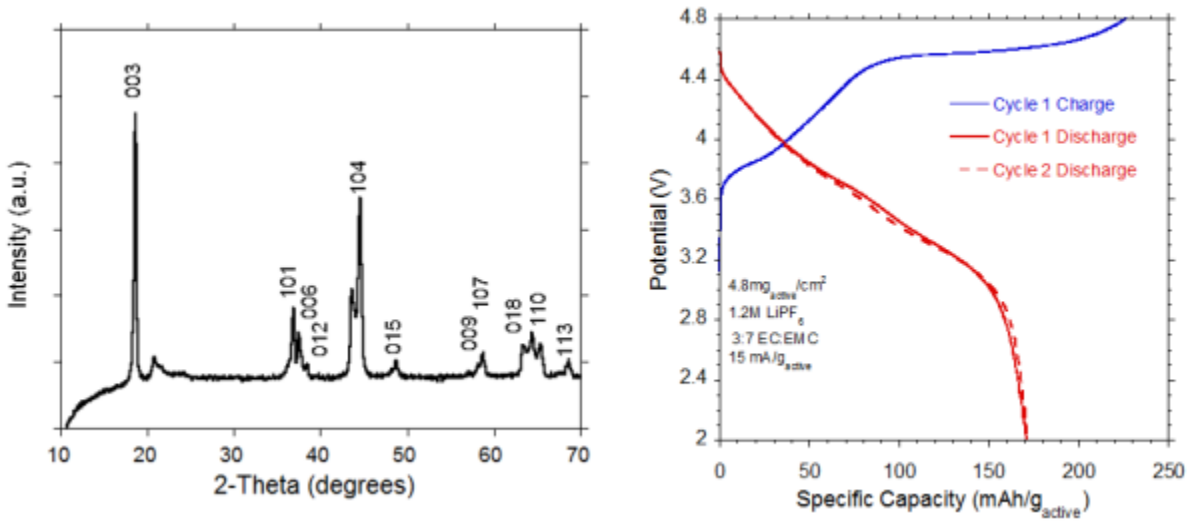

Figure 9. XRD and Voltage curves for the final lithium rich product produced [13, 15]

4.3.2 High Voltage $LiCoO_2$ through $AlPO_4$ Coating

Methods to enable charging to higher voltages are of significant interest to increase commercial cathode voltage and specific capacity to increase energy density. Selected voltage curves over 80-100 cycles for $AlPO_4$ and bare $LiCoO_2$ charged to 4.5 V and 4.6 V are shown in Figure 10. The results demonstrated significantly improved cycling with the $AlPO_4$ coating. The average voltage of $LiCoO_2$ increases to 4.02V and 4.1V when charging to 4.5V and 4.6V respectively. This cathode would exceed NCA in specific energy density when charged to 4.5V and lithium rich materials when charged to 4.6V.

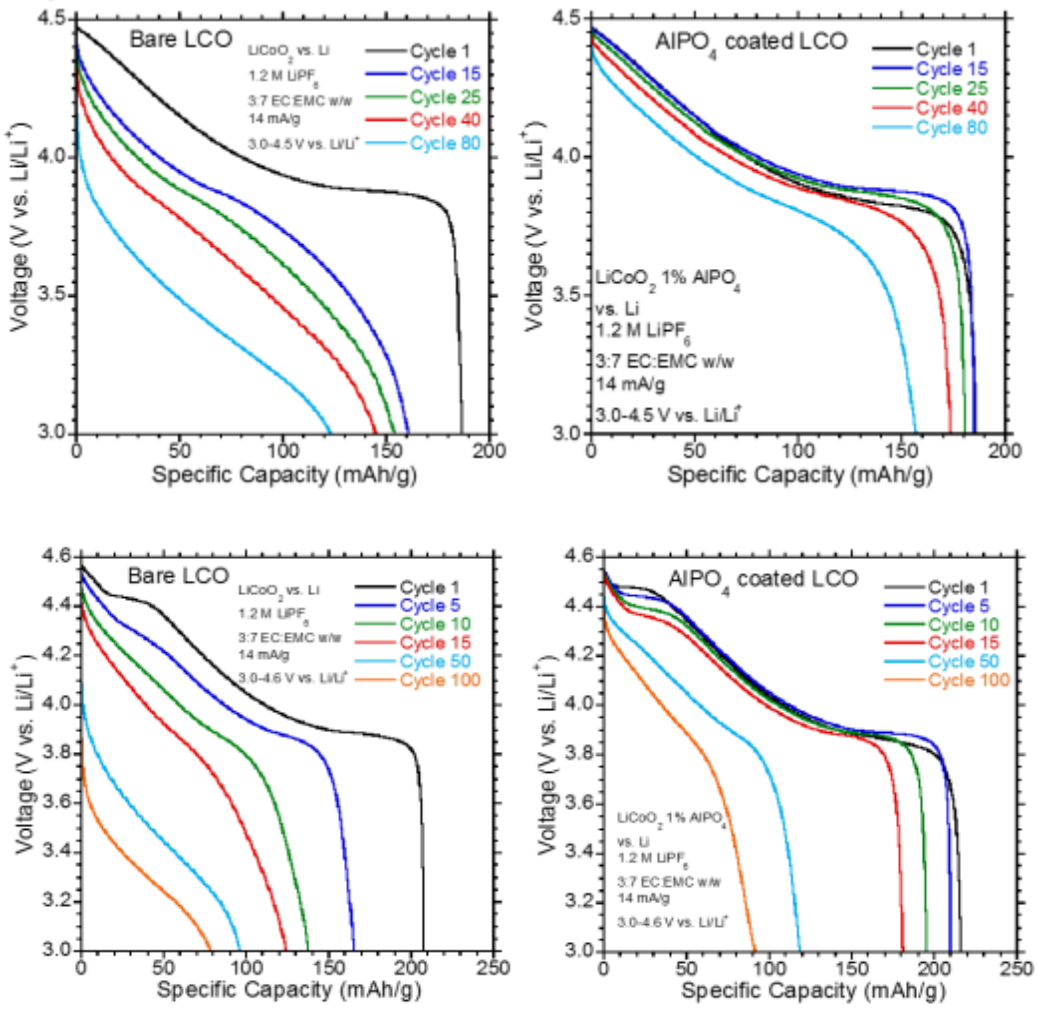

Figure 10. Voltage vs. Specific Capacity for $AlPO_4$ coated and untreated $LiCoO_2$ in standard cathode coatings.

Note: Selected discharge curves over the 80-100 cycles are plotted for 4.5 V charge voltage (top) and 4.6 V charge voltage (bottom)

4.4 Conclusions – Cathodes

A key component to enable higher energy density lithium ion cells are higher specific capacity and voltage cathode materials. The published results from three microsphere papers claimed >300 mAh/g and better cycleablilty than other lithium rich cathode publications. However, following these procedures and several modifications all resulting in similar reversible capacity of ~175 mAh/g. Increasing the cathode charge voltage is an alternative method to greatly increase average voltage and specific capacity. Initial results through $AlPO_4$ coatings of $LiCoO_2$ following a solution based technique are promising to increase cell energy density. Capacities were increased from 150 mAh/g to ~225 mAh/g and voltage increased from 3.6V to 3.9V by allowing a higher charge voltage. Comparison to untreated $LiCoO_2$ material demonstrates significantly better cycling.

5 HIGH CAPACITY ANODES

5.1 Introduction

In the anodes, both the active material and inactive current collector are significant contributors to the mass (and consequently energy density) of the electrode. For the active material, the semiconductor material silicon is a promising anode active materials with theoretical capacity of 4200 mAh g^{-1}. By substituting this high capacity material for conventional graphitic active materials, gains in electrode energy density can be achieved due to active mass reduction. One approach for reducing the mass of the inactive mass is to replace the copper current collector with highly conductive CNTs which can reduce the mass by an order of magnitude. Other potential benefits of replacing copper with CNTs include increased depth of discharge (copper oxidizes below 2.5 V), storage at near-zero volt state of charge, and high temperature applications (>200 °C). Combination of these two approaches (high capacity active materials and alternative current collectors) provides the greatest opportunity for developing anodes with the highest possible capacities.

5.2 Methods – Silicon on CNT Preparation

An Applied Materials P5000 plasma-enhanced chemical vapor deposition system (PECVD) was used to deposit silicon onto sheets of multiwalled carbon nanotube paper from Nanocomp Technologies, Inc. Pure silane gas flowing at 130sccm was used as the source of the silicon. The PECVD was operated at 400°C at a pressure of 3.0 Torr with 75W RF at 13.6MHz. Coating times from 100-1100 seconds were used in increments of 200 seconds. An image of the samples produced in presented in Figure 11 below.

Electrodes were cut out of the silicon on CNT sheets, and incorporated into 2032 coin cells against a lithium metal counter electrode to evaluate the capacity of the material. Samples of the 200s and 1100s deposition were subjected to a further thermal oxidation in a tube furnace in order to remove excess CNT current collector from the sample. Two types of thermal oxidations were attempted – a simple ramp to 560°C at 10°C/min, and a ramp to 560°C followed by a 2 hour hold at that temperature. Both oxidations were carried out under dry air flow. These samples were analyzed via thermogravimetric analysis (TGA, TA Instruments) to gain greater insight into the thermal oxidation process. They were also evaluated in coin cells against lithium metal to determine electrode capacity.

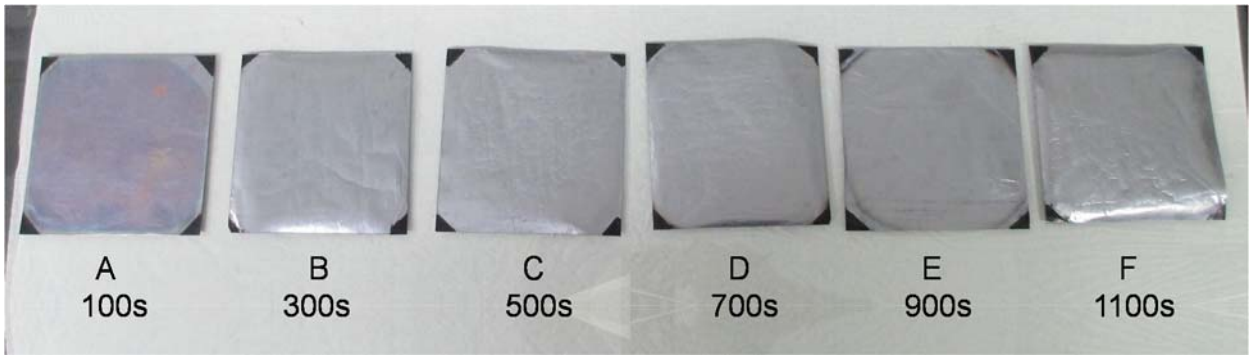

Figure 11. Silicon-on-CNT electrodes produced with various deposition times

5.3 Results and Discussion – Anodes

The 100 second deposition time was somewhat iridescent in appearance, while longer deposition times exhibited a solid silver coloration. SEM images taken as the deposition time increased past 500 seconds, striations from internal strain in the thicker coatings began to appear on the surface of the electrodes, and small particles of silicon were observed to flake off from the electrode. Above this time, there was not observed to be a consistent relationship between the deposition time and coating mass.

SEM images of the electrode with the 100s deposition time revealed a thin conformal coating of silicon that matched closely to the underlying CNT surface. Longer deposition times led to a smoother surface marked with larger spherical features. These images are presented in Figure 12.

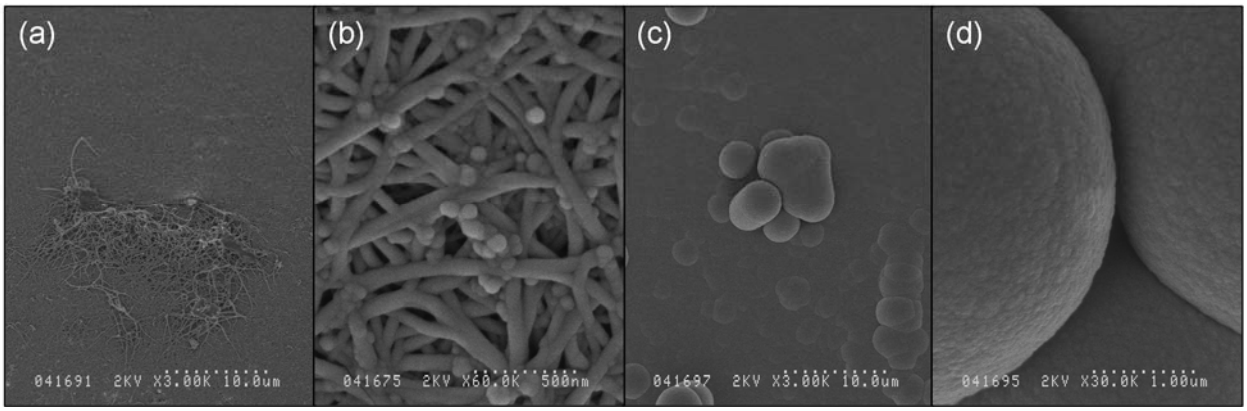

Figure 12. (a) Low and (b) high magnification images of the 100s deposition sample, (c) Low and (d) high magnification images of the 1100s deposition sample

Data from the coin cell cycling showed repeatable extraction capacity after the first cycle. The first cycle coulombic efficiency appeared to be directly correlated with the mass loading of the

silicon, as seen in Figure 13a. The extraction capacity appeared to be inversely correlated with silicon loading, and directly correlated with anode mass, as seen in Figure 13b. The high capacity values at low weight loadings are likely due in part to the underlying capacity of the CNT current collector itself. Overall, the results for extraction capacity and efficiency were comparable to our previously published data [3].

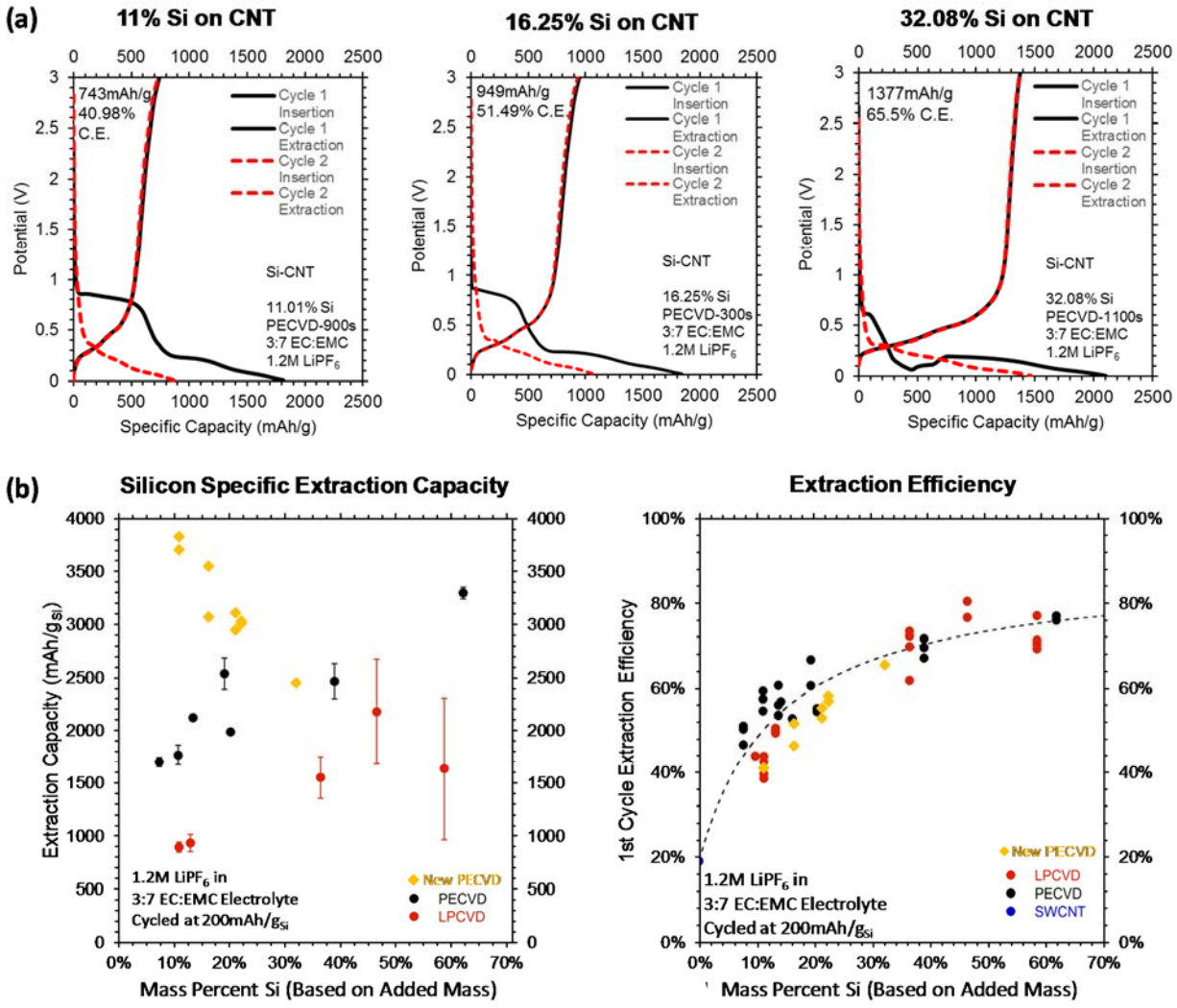

Figure 13. (a) Lithium insertion and extraction cycling profiles for Si on CNT electrodes of various mass loadings, (b) Comparison of extraction capacity with previously published data

Thermogravimetric analysis of the CNT current collector under dry air revealed the presence of two major regions of thermal decomposition. These peaks have previously been assigned to carbonaceous impurities in the sample (lower decomposition temperature) and the CNTs themselves (higher decomposition temperature). In the Si on CNT electrodes the intensity of the major CNT decomposition peak is suppressed and split, as seen in Figure 14a.

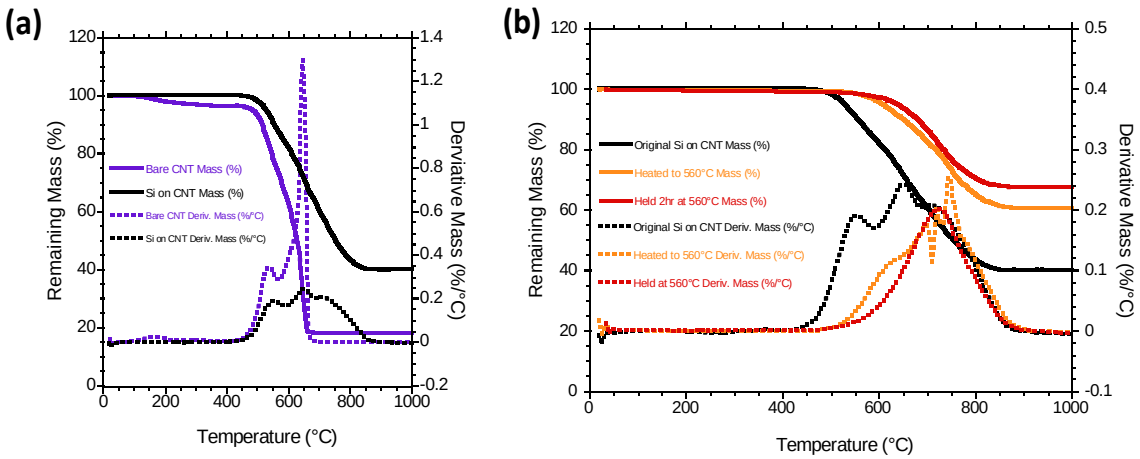

Figure 14. Thermogravimetric analysis data of (a) bare and silicon coated CNTs, (b) thermally oxidized Si on CNT electrodes

The changes in decomposition behavior could be the result of a protecting effect of the silicon coating on the upper portion of the CNT current collector. Thus, higher relative Si mass loading may be obtainable by oxidizing away excess CNT current collector through thermal treatment of the sample. Samples thermally oxidized with the ramp to 560°C exhibited suppression of the carbon impurity peak while still maintaining the two distinct higher temperature decomposition regions around 700°C and 750°C. Samples treated with the ramp to 560°C followed by the two hours hold at temperature exhibited only one major decomposition peak around 725°C. These results can be seen in Figure 14b.

Cycling data from these cells showed capacity increases slightly above the baseline measurements, as can be seen in Figure 15. There was also a significant improvement ratio of the silicon mass to current collector. This data indicates that thermal oxidation treatment is a viable option to increase the active mass fraction of silicon on CNT anodes. However, the silicon coatings did flake off of the electrodes at deposition times longer than 500 seconds. This poses a limit to the utility of PECVD as a method for the production of high areal capacity Si on CNT anodes. The highest areal capacity obtained from this deposition process was approximately 3.1mAh/cm^2 for the 1100 second deposition time.

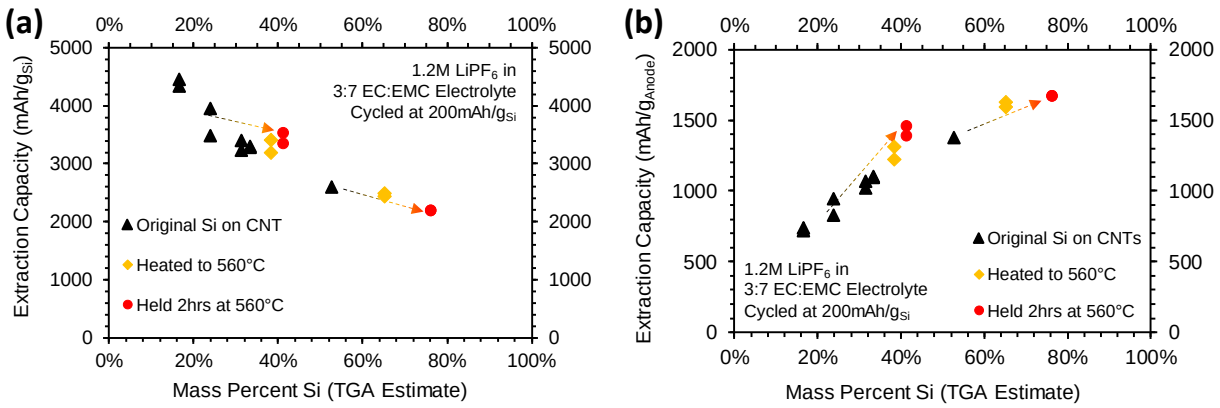

Figure 15. Second cycle lithium extraction capacity based on (a) estimated mass of silicon and (b) total anode mass

5.4 Conclusions - Anodes

Improvement of the energy density of the anodes in lithium-ion cells can best be achieved by a combined approach of using high capacity anodes active materials such as silicon with low density current collectors such as carbon nanotubes. In this study, PECVD was used to deposit silicon onto multi-walled CNT current collector sheets. Through thermal oxidation of the sheets, active mass loadings of up to an estimated 76% were obtained with extraction capacities of 1673mAh/g of anode. Unfortunately, due to internal stresses in the deposited layer, the maximum obtainable areal capacity was only 3.1 mAh/cm^2. To increase this value in future studies, PECVD can perhaps be combined with an initial low pressure chemical vapor deposition (LPCVD) coating of silicon, which deposits deeper into the CNT sheet. Alternately, surface modification of the CNT sheet may be able to obtain better silicon adhesion to the current collector.

6 APPROACHES TO ZERO-VOLT

The sections that follow summarize the efforts regarding development of near zero volt capable lithium ion batteries, including assembly and fabrication, electrochemical testing, and device analysis. These sections contain excerpts from publications which are references [17-18] or work to be published.

6.1 Introduction

As society transitions to renewable energy sources and expanded use of electrical energy, energy storage in a reliable and safe manner is becoming more paramount. For many portable applications, electrochemical energy storage using lithium ion batteries is currently the premier method due to the enhanced rechargeable chemistry. Compared to other designs (i.e. NiCd, Ni-H, etc.) lithium ion has higher energy density, cycle life and highly tunable performance characteristics. There are many efforts underway to enhance lithium ion battery performance to align with future application needs, however, as energy density increases, the associated safety risks also increase.

The safety of lithium ion batteries can be improved when in a user-*inactive* state by application of a resistor to discharge them to a near zero volt, completely discharged state. In a completely discharged, near zero volt state the safety risks associated with lithium ion batteries decreases substantially. Additionally, unlike in lithium ion cells in a mid-range state of charge (i.e. 10-90%) (for which there is currently no method that can rapidly, reliably and accurately determine the state of charge in the field), the near zero voltage of a lithium ion cell with an applied resistor can be easily monitored or checked. Such a capability introduces significant controllability that overcomes the need to trust manufacturers to comply with low state of charge limitations for shipping. Thus, maintaining user-inactive lithium ion cells in a near zero volt state can lead to significant improvements in safety when cells are stored or shipped. However, conventional lithium ion cells are significantly damaged if discharged to a near zero volt state. Several methods to create advanced lithium ion cells that can tolerate a near zero volt or over-discharged state have been pursued, but all involve material substitutions or additions that can lead to increased cell costs, reduced cell performance, operational complications and/or safety concerns. Thus, identification, understanding, and demonstration of a more advantageous way to render advanced lithium ion cells tolerant to a near zero volt state is necessary to improve the future feasibility of maintaining user-*inactive* lithium ion cells in a near zero volt state with an applied resistor to improve their safety during storage or shipping.

During storage or shipment of user-inactive lithium ion batteries, manufacturer defects or abuse of lithium ion cells within a battery can lead to a thermal runaway event. Thermal runaway results from several internal exothermic reactions that are initiated by overheating of a cell that can result from internal short, rapid charge/discharge, overcharge, external heating, or other abuse condition. The exothermic reactions include Solid Electrolyte Interface (SEI) decomposition, electrolyte reaction with the electrodes, decomposition of active materials and electrolyte decomposition. Thermal runaway can result in a dangerous fire or explosion that can propagate to other nearby cells. In the case of a large battery consisting of many lithium ion cells, or many batteries stored together, propagation can lead to a very dangerous event with

severe damage including explosion, fire, and venting of toxic gases. Several research efforts to mitigate safety risks while lithium ion batteries are in a user-*active* state have been reported. Internal to lithium ion cells, shut-down separators to prevent ion flow upon overheating, cathode coatings to suppress exothermic release, non-flammable electrolytes to avoid electrolyte combustion and redox shuttle additives to prevent overcharge have been investigated. External to cells during normal operation, battery management systems (BMS) to avoid abuse of cells, blocking diodes to prevent inadvertent charge or discharge, current limiting fuses to prevent rapid charge or discharge, and bypass diodes to prevent overcharge/overdischarge of a "weak" cell in a battery pack have all been investigated or are currently used. In the case of entering dangerous operating conditions, positive temperature coefficient devices (PTCs) to block or reduce current upon overheating and current interrupt devices (CIDs) to block current in the case of over-pressure have been used or are currently in use.

6.2 CNT Paper Current Collectors

Increasing the gravimetric energy density of lithium ion batteries has been a large focus of research in recent years. Increased gravimetric energy density can have many benefits in aerospace, electric vehicle (EV) and portable electronics applications. Among several approaches to increasing the gravimetric energy of lithium ion batteries, including thicker composites, more energy dense cathode active materials and high capacity alloying anode materials, using carbon nanotube papers as a lightweight current collector replacement, particularly as a replacement for the copper foil of the anode, has been investigated.

Carbon nanotube papers have several advantages over standard copper foils. In particular they are roughly an order of magnitude lower areal density and they can contribute up to 100 mAh/g capacity in the 0.005-1.5 V vs. Li/Li^+ potential range. Carbon nanotube papers are also very stable to high potentials (>3.0 V vs. Li/Li^+) and when used as the anode current collector could enable lithium ion cells that can withstand over-discharge or prolonged storage at a near zero volt state of charge. Carbon nanotube papers can also form a mechanically compliant current collector for materials like silicon and germanium thin films, leading to better performance. However, carbon nanotube papers are known to suffer significant first cycle loss due substantial SEI formation caused by their high surface area. The carbon nanotube bundles that make up a CNT paper also suffer reduced packing density after repeated cycling which could affect the electrical conductivity of the CNT papers. Generally, pathways to reduce SEI formation on CNT papers and improved cycling stability are necessary to improve the utility of CNT papers as an effective anode current collector replacement for copper foils.

6.3 Reversible Lithium Management

If lithium ion cells could be modified in such a way that complete discharge to a near zero volt state of charge did not damage internal components, the motivation of rendering lithium ion batteries safe to transport and resolving both the implementation challenge of state-of-charge limitations and over discharge risk could be realized. In a representative scenario, after a cell is discharged to a low state of charge, an appropriately sized resistor (i.e. won't discharge the cell too rapidly or too slowly) can be applied to the cell to further discharge it towards the ideal case of no stored charge energy and a cell voltage of near zero volts. The very low state of charge will increase safety of the cell by increasing onset temperatures of exothermic reactions and

preventing a rapid discharge resulting from an internal or external short (due to near zero potential difference between the electrodes). Additionally, the state of charge could be easily checked by a handheld voltmeter since the cell voltage will be near zero volts. Thus, discharging and storing lithium ion cells at a near zero volt state of charge has the potential to significantly decrease associated safety risks and allow for highly controllable implementation of a state of charge restriction on lithium ion batteries that are to be transported or stored.

The key to implementing such a promising approach in the near future is to accomplish near zero volt storage resilience of lithium ion cells with little to no modification to a conventional design. This would be a stark contrast to past approaches that require modifications to cell design and use of unconventional materials that can reduce cell quality and performance while increasing cost. The copper current collector is the primary degradation component when a full cell is discharged to zero volts. The copper will dissolve at voltages below ~1.0V in a full cell due to the dissolution potential vs. lithium reaching >1.5V. However, this work will show that pre-lithiation of the anode with reversible excess lithium can prevent the anode from reaching the copper dissolution potential and allow current cell designs to be zero-volt capable.

7 CNT CURRENT COLLECTORS FOR ZERO-VOLT

Al2O3 coating of CNT paper current collectors

In the present work, a ~3 nm layer of Al_2O_3 is deposited by atomic layer deposition onto commercial CNT papers and its effect on the lithium ion cycling performance of the CNT papers is investigated. Cycling of the CNT papers vs. Li metal in coin cells is used to investigate charge loss, specific capacity and cycling stability of CNT papers. X-ray diffraction is used to investigate the effect of the Al_2O_3 coating on maintaining bundle packing (crystallinity) of the CNT papers during cycling. Raman spectroscopy is used to investigate the effect of the Al_2O_3 coating on defect creation in the CNT's during cycling. Lastly, a MesoCarbon MicroBead (MCMB) anode composite is coated onto the CNT paper and the electrode is tested by cycling vs. Li metal in a coin cell to determine the viability of an Al_2O_3 coated CNT paper as a current collector replacement.

7.1 Experimental

Purification and Al_2O_3 coating of commercial MWCNT sheet material

The processing steps performed on the commercial multiwall carbon nanotubes (MWCNT) sheet materials obtained from Nanocomp Technologies Inc. are shown in the flowchart in Figure 16. As-received MWCNT sheet material first underwent a thermal oxidation (Ramp-stop from room temperature to 520°C at 10°C/min under flowing dry air) to remove amorphous carbon material which thermally oxidizes at a lower temperature than MWCNT's. The sheet material was then immersed in regent grade HCl for 30 minutes to remove residual metal catalyst left over from the material synthesis. The material was then rinsed with excess DI H_2O and dried before undergoing another thermal oxidation (Ramp-stop from room temperature to 520°C at 10°C/min under flowing dry air) to remove residual HCl from the material.

Following purification the aluminum oxide (Al_2O_3) coatings were grown at 125°C by atomic layer deposition (ALD) in a commercial Beneq TFS-200 system. The MWCNT sheet was suspended inside the reactor to create a gap between the substrate holder and the bottom surface of the MWCNT sheet, to ensure that both the top and bottom sides are conformally coated with ~3 nm Al_2O_3. The precursors used were trimethylaluminum (TMA, $Al(CH_3)_3$) and deionized H_2O for the aluminum and oxygen sources, respectively, and both precursors were kept at 20°C. Ultra-high purity argon (UHP Ar) was used as the carrier gas. Since MWCNT's have a relatively inert surface, water was pulsed first to help with TMA nucleation. Thus, the ALD sequence consisted of the following: H_2O / UHP Ar / TMA / UHP Ar. The exposures for both precursors were 0.15 s, and the purge times were 5 s and 1 s for H_2O and TMA, respectively. The coating thickness targeted was 3 nm based on tool calibration. A prior study has shown that atomic layer deposition onto MWCNTs with similar deposition conditions and distilled H_2O and TMA as pre-cursors leads to a conformal coating of an amorphous Al_2O_3 layer. The Al_2O_3 coated MWCNT paper will be referred to as Al_2O_3-MWCNT paper hence forth.

Electrochemical Testing

Electrodes were built into 2032 coin cells vs. lithium metal with a Celgard separator between them for electrochemical testing. The electrolyte used was a 1.2 M $LiPF_6$ in 3:7 EC:EMC w/w. Cells were constructed in a dry, Argon filled glove box maintained at <1% Oxygen and <1% water. Cycling was performed on an Arbin BT2000 cycler.

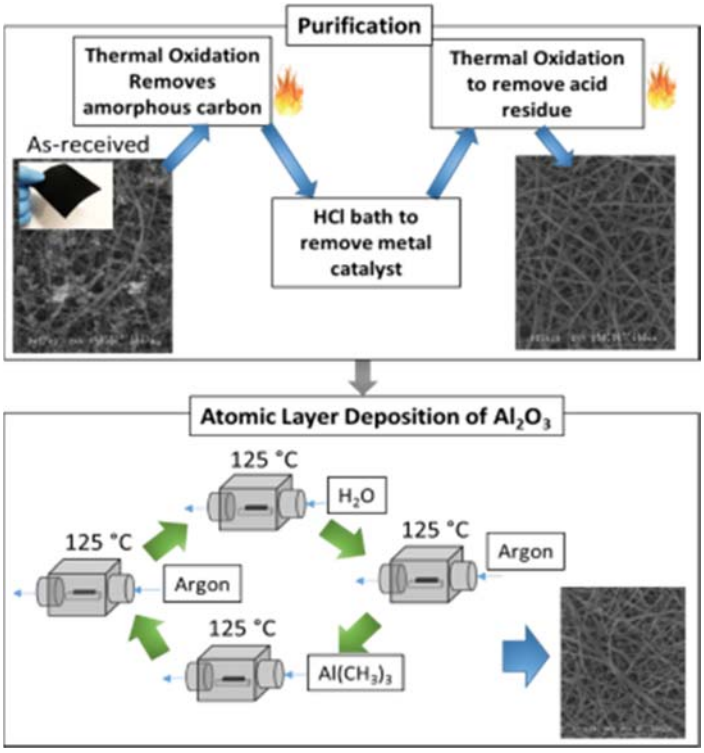

Figure 16. Flow diagram of processing steps of commercial MWCNT sheet materials to remove amorphous carbon and residual metal catalyst and coated with ~3 nm of Al_2O_3

MCMB composite electrode fabrication

Mesocarbon microbead (MCMB) composite anodes coated onto MWCNT paper current collectors were prepared by mixing Quallion 25-28 (T13E00-1)) MCMB into a slurry with SuperC™ Carbon Black, TIMREX® synthetic flake graphite from TIMREX® (SFG-6) and Solef® PVDF in a 93:0.3:2.7:4 mass ratio using NMP as the solvent. The slurry preparation consisted of dissolving PVDF in NMP, then by mixing in the conductive additives (Carbon Black and SFG-6) and then addition of the MCMB with intermediate mixing steps in a Thinky AR-100 planetary mixer. The composite slurry was coated onto the MWCNT paper using a doctor blade. The electrode was then dried overnight in a vacuum oven at 100°C and calendared to a composite density of about 1.39 g cm^{-3}. The final electrode areal density was 15±1 mg/cm^2.

Cell disassembly and electrode rinsing

2032 coin cells were disassembled in a dry, Argon filled glove box maintained at <1% Oxygen and <1% water using a de-crimping tool. The CNT paper electrodes were rinsed in excess EMC and dried in vacuum for 2 hours before analysis.

Material Analysis

Raman spectroscopy was performed using a Jobin Yvon LabRam spectrophotometer with a 633 nm light source and 300 to 3000 cm^{-1} collection range. X-ray diffraction (XRD) was performed with a Bruker D2 Phaser powder x-ray diffractometer. A Cu kα 1.54184 Å x-ray source was used. The step size was set to 0.0081167 (2θ) with 1 second collection time at each step. The electrode was placed on a sample holder that was rotated at a rate of 1.0 rotation/second. Background subtraction and smoothing was done using Bruker Diffrac software.

7.2 Results and Discussion

The first cycle insertion of lithium into a bare MWCNT paper and an Al_2O_3-MWCNT paper is shown in Figure 17a. As shown, the voltage profile of the bare MWCNT paper has a plateau at about 1.0 V vs. Li/Li^+ that extends out to ~1500 mAh/g insertion specific capacity. This plateau is attributed to SEI formation on the MWCNT paper and is substantial due to the high surface area of the MWCNTs. After 1500 mAh/g_{CNT} of insertion capacity, the voltage decreases to 5.0 mV vs. Li/Li^+ after an additional 1200 mAh/g_{CNT} insertion specific capacity, resulting in total first cycle insertion specific capacity of 2800 mAh/g_{CNT}. In comparison, the voltage profile of the MWCNT paper coated with Al_2O_3 is very different. Compared to the bare CNT paper, the insertion specific capacity of the plateau observed at ~1.0 V vs. Li/Li^+ is significantly reduced by about 75% to ~500 mAh/g_{CNT}. After 500 mAh/g_{CNT} of insertion specific capacity, the potential of the AL_2O_3-MWCNT paper decreases to 5 mV vs. Li/Li^+ after an additional 500 mAh/g_{CNT} of insertion specific capacity, resulting in a total first cycle insertion capacity of 1000 mAh/g_{CNT}.

The decrease in specific insertion capacity at the ~1.0 V vs. Li/Li^+ plateau of MWCNT coated with Al_2O_3 compared to pristine MWCNT is attributed to a significant decrease in SEI formation on the MWCNT paper. Al_2O_3 coatings have resulted in a decrease in SEI formation in Si anodes as well. Significant SEI formation during the first cycle is a major challenge of MWCNT papers as anode current collector replacements in lithium ion batteries. Thus, such a significant reduction of the amount of SEI formation can have a substantial impact on the feasibility of using MWCNT papers as an anode current collector replacement.

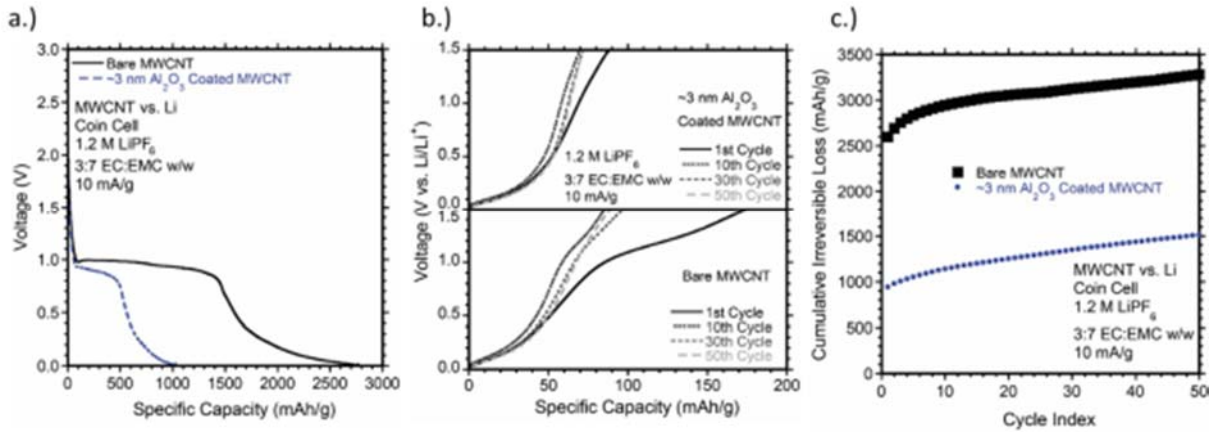

Figure 17. (a) First cycle insertion of lithium into CNT paper electrodes, (b) Cumulative irreversible loss plotted against cycle index for a CNT paper electrode coated with Al_2O_3 and a bare CNT paper electrode, (c) Extraction voltage profile of (top) Al_2O_3 coated CNT paper electrode and (bottom) bare CNT paper electrode

Figure 17b shows the 1st, 10th, 30th and 50th cycle extraction voltage profiles of the bare MWCNT paper and an Al_2O_3-MWCNT paper. The 1st cycle voltage profile of the bare MWCNT shows 170 mAh/g_{CNT} extraction specific capacity, with pseudo-plateaus at ~0.2 mV vs. Li/Li^+ and ~1.2 V vs. Li/Li^+, similar to a previous study on single walled carbon nanotube papers. The 10th cycle voltage profile of the bare MWCNT shows a significant decrease in the pseudo-plateau at ~1.2 V vs. Li/Li^+ compared to the 1st cycle which decreases the extraction capacity to 90 mAh/g_{CNT}. In the 30th cycle the small remnant "shoulder" feature of the profile at ~1.2 V vs. Li/Li^+ has decreased more and during the 50th cycle is no longer present.

By comparison, the 1st cycle extraction voltage profile of the MWCNT coated with Al_2O_3 profile has only a pseudo-plateau at ~0.2 V vs. Li/Li^+ with a 90 mAh/g_{CNT} extraction capacity. The 10th cycle voltage profile is very similar, with the extraction capacity decreasing by about 20 mAh/g_{CNT} to 70 mAh/g_{CNT}, with the decrease in overall extraction capacity resulting from a decrease in extraction at potentials >0.5 V vs. Li/Li^+. The 30th and 50th cycle extraction voltage profiles of the Al_2O_3 coated CNT paper are nearly identical to that of the 10th cycle, indicating stable cycling.

The decrease in the magnitude of the ~1.2 V vs. Li/Li^+ pseudo-plateau with cycle index in the bare MWCNT paper electrode is consistent with repeated stripping of unstable SEI components followed by re-deposition of new SEI during each insertion step until only stable components of the SEI are present. The absence of the pseudo-plateau in the first cycle extraction voltage profile of the Al_2O_3-MWCNT paper indicates the Al_2O_3 promotes growth of an SEI layer with more stable components during the initial insertion step.

Figure 17c shows the cumulative irreversible loss of the bare MWCNT electrode and Al_2O_3-MWCNT electrode plotted as a function of cycle index. As shown, after 50 cycles the cumulative irreversible loss of the Al_2O_3 coated electrode is about 45% of the cumulative

irreversible loss of the bare MWCNT electrode. Thus, after 50 cycles, the Al_2O_3 coating effects a greater than 50% decrease in irreversible losses exhibited by a MWCNT paper electrode.

Figure 18 shows the X-ray diffraction spectra of bare and Al_2O_3-MWCNT papers before electrochemical cycling (top) and after electrochemical cycling (bottom). As shown in the top of the diagram, a peak appears at about 25 degrees (2-theta) which corresponds to the inter-MWCNT spacing in MWCNT bundles which is roughly the same as graphene plane spacing in graphite. As shown in the top of Figure 18, the peak shape and intensity relative to noise is very similar in the bare MWCNT paper and the Al_2O_3-MWCNT paper, indicating the bundling of MWCNTs in each sample is very similar. Thus, the Al_2O_3 coating process did not affect the bundling of CNTs in the coated samples.

The bottom part Figure 18 shows the XRD pattern of the CNT paper electrodes after the cycling shown in Figure 17. As shown, the peak at about 25 degrees (2-theta) is no longer present for the bare MWCNT paper, indicating that in the CNT bundles individual CNT's are no longer packed together with the graphene spacing distance separating them. For the Al_2O_3-MWCNT paper, the peak is still present, but its intensity relative to noise appears to have decreased while its width has slightly increased. The presence of the peak indicates that in the bundles of the MWCNT electrode, individual CNT's are packed with the graphene spacing distance separating them. Thus, the Al_2O_3 coating has maintained the bundle packing of CNTs during cycling of the-MWCNT paper electrode to greater extent than is observed in the bare MWCNT paper electrode.

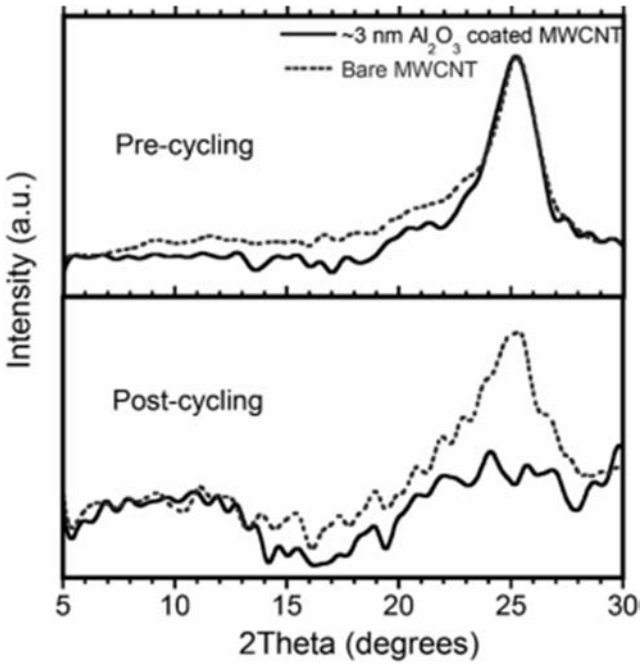

Figure 18. XRD pattern of the bare MWCNT and Al_2O_3-MWCNT before cycling (top) and after cycling (bottom)

Figure 19a shows the Raman spectra of bare MWCNT paper prior to the cycling shown in Figure 17 (bottom) and after cycling (top). As shown, peaks appear at 1320 cm^{-1}, 1600 cm^{-1} and 2640 cm^{-1}. The peak at 1600 cm^{-1} (G-peak) corresponds to longitudinal and latitudinal vibrations of the graphene sub-lattices that make up the concentric walls of the MWCNTs. The peak at 1320 cm^{-1} (D-peak) corresponds to scattering with a defect site in a cylindrical graphene layer of the MWCNT such as a vacancy or displacement. The peak at 2640 cm^{-1} (G' peak) corresponds to two photons, 2nd order scattering process. As shown in Figure 19a, after cycling the magnitude of the D-peak relative to the G-peak and G' peak has increased significantly compared to the sample prior to cycling (D/G ratio 0.2 -> 0.9). The increase in the relative intensity of the D-peak indicates that cycling has increased the density of defect sites in the walls of the MWCNTs, as observed in prior work. By comparison, in the coated Al_2O_3 the relative intensity of the D-peak increases to a lesser extent (0.2->0.8), indicating the density of defect sites is less in the Al_2O_3-MWCNT paper electrode after cycling compared to the bare MWCNT paper electrode. Thus, the Al_2O_3 coating on the MWCNT paper effects a decrease in the creation of defects in the walls of the CNTs during cycling vs. Li metal.

Electrochemical rate capability testing

A second set of 2032 coin cells with MWCNT paper electrodes vs. Li metal were constructed to test the effect of Al_2O_3 coatings on the extraction rate capability of the MWCNT paper electrodes. The cells were cycled 5 times 0.005-1.5 V vs. Li/Li^+ at 15 mA/g_{CNT} to condition the paper electrodes. Then, the insertion rate was held at 15 mA/g_{CNT} and the extraction rate was varied to 15 mA/g_{CNT}, 30 mA/g_{CNT}, 75 mA/g_{CNT}, and 150 mA/g_{CNT}. Figure 20 shows the extraction voltage profiles of Al_2O_3 coated (top) and bare (bottom) MWCNT paper electrodes at the different extraction rates.

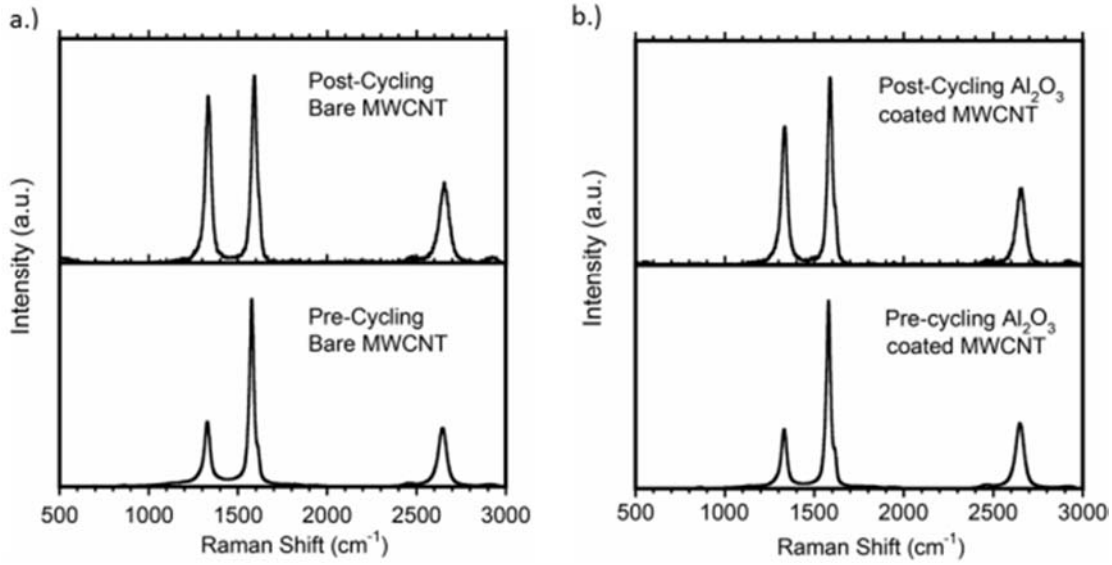

Figure 19. (a) Raman spectra of bare MWCNT before cycling (bottom) and after cycling (top) vs. Li metal in a coin cell, (b) Raman spectra of Al_2O_3-MWCNT before cycling (bottom) and after cycling (top) vs. Li metal in a coin cell

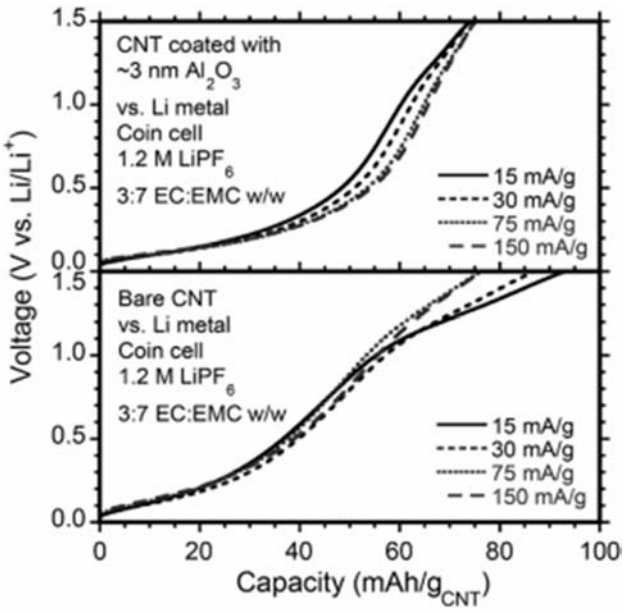

Figure 20. Voltage profile of lithium extraction from Al_2O_3-MWCNT (top) and bare MWCNT (bottom) at 15 mA/g, 30 mA/g, 75 mA/g and 150 mA/g

As shown in the top part of Figure 20, the extraction voltage profile of the Al_2O_3-MWCNT paper electrode changes little at the different extraction rates up to an effective 2C extraction rate. By comparison, the extraction voltage profile of the bare MWCNT paper electrode also has no notable change at the different extraction rates up to an effective 2C extraction rate. The change in the extraction profile above 1.0 V vs. Li/Li^+ is likely attributed to continued conditioning of the SEI layer as shown in Figure 17b. Overall, the results show that the Al_2O_3 coating does not negatively affect the extraction rate capability of the MWCNT paper electrode up to and effective 2C extraction rate.

MCMB composite was coated on bare MWCNT paper and Al_2O_3-MWCNT paper and testing in coin cells vs. Li metal. The primary purpose of the testing was to evaluate the effect of the thin insulating Al_2O_3 on the performance of a MWCNT paper as a current collector replacement. MCMB vs. Li cells were cycled 5 times from 0.005-1.5 V vs. Li/Li^+ at 15 $mA/g_{electrode}$. Figure 21a shows the first cycle insertion of the MCMB on MWCNT (bare and Al_2O_3 coated) current collectors. As shown, the initial insertion curve from ~0.7 V vs. Li/Li^+ to 0.12 V vs. Li/Li^+ extends to about 60 $mAh/g_{electrode}$ for the MCMB on an Al_2O_3-MWCNT current collector compared to 80 $mAh/g_{electrode}$ for MCMB coated on a bare MWCNT current collector. The decrease in insertion capacity in the ~0.7-0.12 V vs. Li/Li^+ in the electrode with an Al_2O_3-MWCNT current collector can be attributed to the Al_2O_3 coating effecting a decrease in the amount of SEI formed on the electrode.

Figure 21b shows the extraction voltage profile of the MCMB coated on Al_2O_3-MWCNT (top) and bare MWCNT (bottom). As shown, the extraction capacity of both electrodes increases throughout the 5 conditioning cycles. The extraction capacity of the MCMB coated on Al_2O_3-MWCNTs increased from 215 to 284 $mAh/g_{electrode}$. The extraction capacity of the MCMB

coated on bare MWCNT increased 246 to 286 mAh/$g_{electrode}$. The larger change in extraction capacity in the MCMB coated on Al_2O_3 coated electrode may reflect the need to condition the Al_2O_3 layer with partial Li ion insertion before it forms an effective connection to the MCMB composite. Overall, after 5 conditioning cycles, the extraction capacity of both electrodes is nearly identical. Thus, the Al_2O_3 coating on the MWCNT current collector does not diminish the available capacity of a composite coated on it.

Figure 21c shows the cumulative irreversible loss for the first 5 conditioning cycles of the MCMB coated on Al_2O_3-MWCNT and bare MWCNT current collectors. As shown, the cumulative irreversible loss after 5 cycles is 96 mAh/$g_{electrode}$ for the MCMB coated on Al_2O_3-MWCNT current collector and 115 mAh/$g_{electrode}$ for the MCMB coated on a bare MWCNT current collector. The ~17% decrease in cumulative irreversible loss in the anode with a Al_2O_3-MWCNT current collector can be attributed to a reduction in the SEI formation on the CNTs as shown in Figure 17. Thus, an Al_2O_3 coating on a MWCNT current collector decreases irreversible losses of electrodes during conditioning.

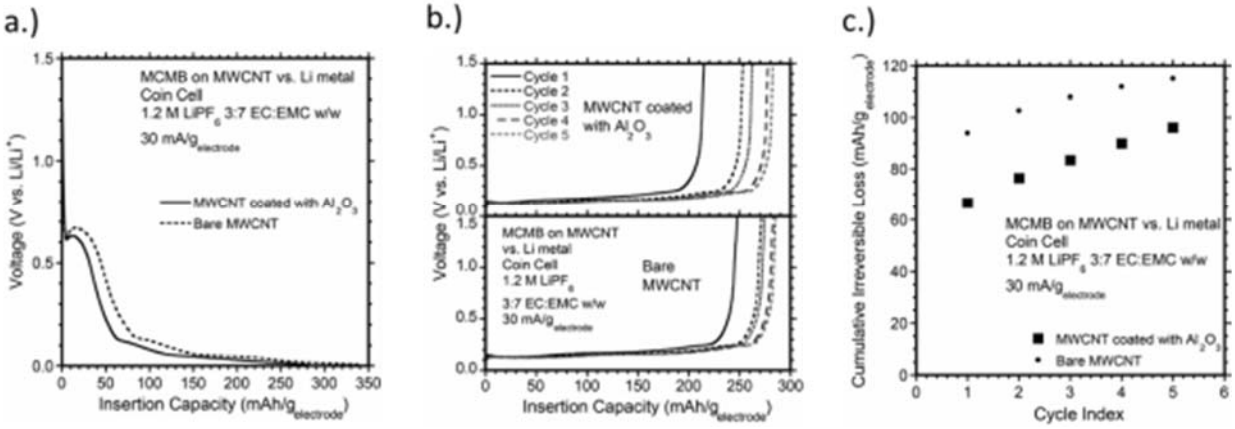

Figure 21. (a) First cycle insertion voltage profiles of MCMB composite coated onto bare MWCNT or Al_2O_3-MWCNT, (b) Extraction voltage profiles for cycles 1-5 of MCMB composited coated onto Al_2O_3-MWCNT (top) and MCMB composite coated onto bare MWCNT (bottom), (c) Plot of cumulative irreversible loss as a function of the cycle number for MCMB composite coated onto bare MWCNT or Al_2O_3-MWCNT

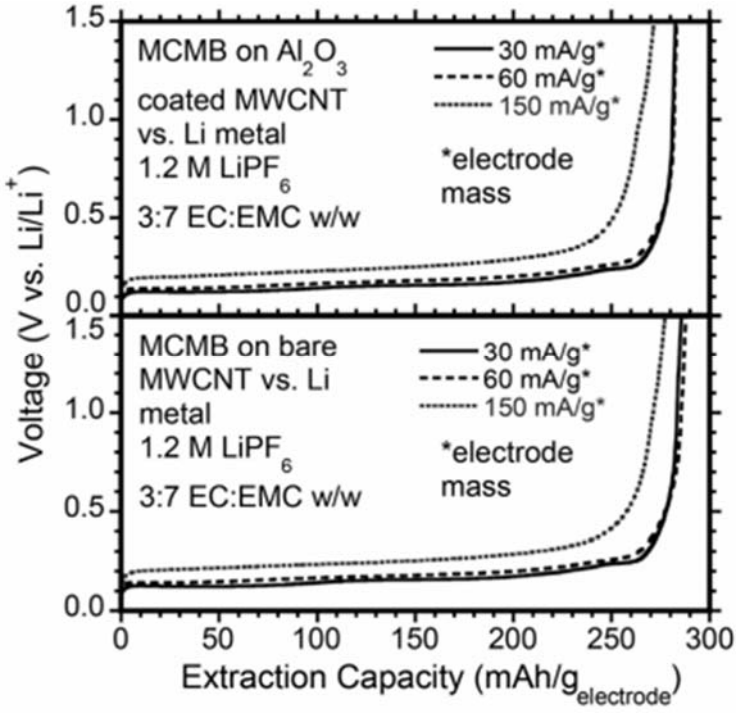

Figure 22. Extraction voltage profiles at rates of 30, 60 and 150 mA/$g_{electrode}$ of MCMB composited coated onto Al_2O_3-MWCNT (top) and MCMB composite coated onto bare MWCNT (bottom)

After conditioning, the MCMB coated on Al_2O_3-MWCNT current collector and bare MWCNT current collector underwent an extraction rate study in which the insertion rate was held constant at 30 mA/$g_{electrode}$ and the extraction rate was changed to 30 mA/$g_{electrode}$ (~C/10) to 60 mA/$g_{electrode}$ (~C/5) and 150 mA/$g_{electrode}$ (~C/2). As shown in Figure 22, for each tested rate the voltage profile of the MCMB coated onto Al_2O_3-MWCNT is nearly the same as the voltage profile of the MCMB coated on bare MWCNT. Thus, the Al_2O_3 coating on the MWCNT paper does not affect charge transfer processes between the MWCNT current collector and MCMB composite in a manner detrimental to extraction rate capability.

7.3 Conclusions

The electrochemical performance of a MWCNT paper electrode coated with ~3 nm of Al_2O_3 by atomic layer deposition was characterized and compared to that of a bare MWCNT electrode. Cycling of the MWCNT paper electrodes vs. Li metal in coin cells showed a significant decrease in SEI formation on the first cycle. Additionally, the voltage profiles over 50 cycles suggests that the Al_2O_3 coating effects the deposition of more stable SEI during the first insertion. Overall, cumulative irreversible loss after 50 cycles was decreased by 55% in the Al_2O_3-MWCNT paper compared to the bare MWCNT paper. XRD analysis indicates that the Al_2O_3 coating maintains the packing of individual MWCNT's in CNT bundles at the graphene separation distance after 50 cycles. Raman spectroscopy shows that the Al_2O_3 coating effects minor suppression of defect

formation in the graphene walls of the MWCNTs. Coating Al_2O_3 coated and bare MWCNT paper electrodes with an MCMB composite shows that the Al_2O_3 reduces the cumulative irreversible loss of the MCMB-MWCNT electrode by ~17% after 5 cycles and does not diminish the rate capability of the MCMB-MWCNT electrode. Overall, the present results suggest coating of CNT paper electrodes with thin oxide materials by atomic layer deposition can improve on the irreversible losses observed with CNT materials when cycled in lithium ion cells. With optimization, ALD coatings of thin oxides may improve the viability of CNT papers as current collector replacements.

8 REVERSIBLE LITHIUM MANAGEMENT

8.1 Introduction – Zero-Volt

Anode pre-lithiation does not introduce unconventional materials or necessitate change in the battery construction parameters, so such an approach can avoid the anticipated trade-offs of the current and past approaches to near zero volt storage tolerance. Additionally, anode pre-lithiation in concept could be applied to a range of difference active material combinations, since there are no operational concerns related to secondary active material stability or reactions with the primary active material.

Pre-lithiation of a graphite anode has also been shown to have the additional benefit of improving performance of conventional cells which can help to reduce the cost/benefit ratio. Also, it may eliminate the need for formation cycling, which could serve to reduce manufacturing costs. Thus, addition of anode pre-lithiation to the battery manufacturing process may not substantially increase the cost of lithium ion cells and could improve general performance in addition to enabling near zero volt storage tolerance.

Additionally, several methods of pre-lithiation with potential for industrial scalability exist. Use of Stabilized Lithium Metal Powder (SLMP) has been shown to be an effective way to pre-lithiate anodes. Electrochemical pre-lithiation such as bath pre-lithiation has also been developed and is a promising option that is scalable. Therefore, industrially scalable pre-lithiation methods exist and could be utilized for large scale production.

For a conventional $LiCoO_2$/graphite cell, after 5 conditioning cycles, a fixed load of 2.5 kOhm was applied to the cell by an Arbin cycler to simulate a resistor placed between the leads of the cell, similar to what could be achieved in a practical storage or transportation situation. The value of the applied load was designed so that at 3.0 V cell voltage, the initial current would be equivalent to a C/10 (1.2 mA) discharge rate. The fixed load step was applied for a total of three days to represent an extended period of near zero volt storage. The benefit of this demonstration is to show the details of cell degradation when it is stored at near zero volts under fixed load.

Three-electrode data for the 5^{th} cycle during discharge is shown as a function of discharge capacity in Figure 23a and as a function of time in Figure 23b. As shown in Figure 23a and b, during the C/10 discharge (first ~12 mAh or ~10 hours) the cell current is constant and the electrode potentials exhibit their normal discharge behavior. At ~12 mAh, (~10 hours), the cell reaches 3.0 V and the fixed load (2.5 kOhm) step is initiated and the cell undergoes a transient period as it discharges to near zero volts. As shown in Figure 23b, the cell voltage decreases to <0.4 V in the first hour which under the fixed load corresponds to a cell current of <0.16 mA. During the first hour, the cathode potential decreases initially, but then recovers to ~3.6 V vs. Li/Li^+ while the anode potential increases rapidly up to ~3.4 V vs. Li/Li^+. Both electrodes plateau at these potentials for ~2 hours. The cathode then decreases and asymptotes to within 10 mV of anode potential at ~3.2 V vs. Li/Li^+. Once the cell reaches this point, the cell voltage is <10 mV and the cell current is <4 μA (C/3000) which is considered to be a quasi-equilibrium state. The quasi-equilibrium state remains for the final 66 hours of the fixed load step. The

electrode potentials slightly decrease during this time by about 0.1 V to ~3.1 V vs. Li/Li^+ and the cell voltage decreases to ~3 mV. Over the course of the 3-day fixed load step, the cell discharged an additional ~0.5 mAh.

The initial decrease and subsequent recovery of the electrochemical potential of the cathode during the transient period may not be expected, but similar results have been observed in prior work. The decrease and recovery of the cathode potential may be due to several non-ideal effects such as changing ionic activities, the effects of reaction rate constants or non-faradaic processes as the cell current decreases. Regardless, the cathode potential remaining in its normal range for several hours and intercalating 0.5 mAh of additional lithium at ~3.6 V vs. Li/Li^+ during the fixed load step supports that the cathode can still intercalate more lithium in its normal potential range after the normal discharge. The rapid rise in potential of the anode when the fixed load is applied is consistent with the anode being mostly depleted of intercalated lithium ions and highly polarizable at the end of discharge. The major concern with the rise in anode potential is the onset of copper dissolution of the copper into the electrolyte can occur as depicted in Figure 23c.

Figure 23d quantifies the copper dissolution process in a linear sweep voltammogram, which uses a polished copper working electrode, polished platinum counter electrode and lithium reference electrode. A Princeton Applied Research Versastat 3 was used for the voltammetry and swept the potential of the copper foil in the positive direction at 10 mV/s from the open circuit voltage (OCV) of ~3.1 V vs. Li/Li^+. As can be seen, an oxidative current from copper foil initiates at a potential of ~3.1 V vs. Li/Li^+ and reaches current densities of ~0.01 mA/cm^2 at 3.3 V vs. Li/Li^+, ~0.1 mA/cm^2 at 3.4 V vs. Li/Li^+ and ~1.0 mA/cm^2 at 3.5 V vs. Li/Li^+. The oxidative current is primarily attributed to copper ions stripping off the surface of the copper foil resulting in soluble cations, consistent with previous studies.

It is important to note here that determined values of the onset potential for copper dissolution can vary since the choice of an oxidative current density threshold is arbitrary and non-faradaic process can contribute to the oxidative current. Additionally, the exact value of the onset of copper dissolution can be affected by factors such as ambient conditions and electrolyte composition. In the present work, 3.1 V vs. Li/Li^+ is assigned for interpretation purposes as below this value, no oxidative current was observed in the linear sweep voltammogram in Figure 23d, and therefore, no copper dissolution is expected to be occurring.

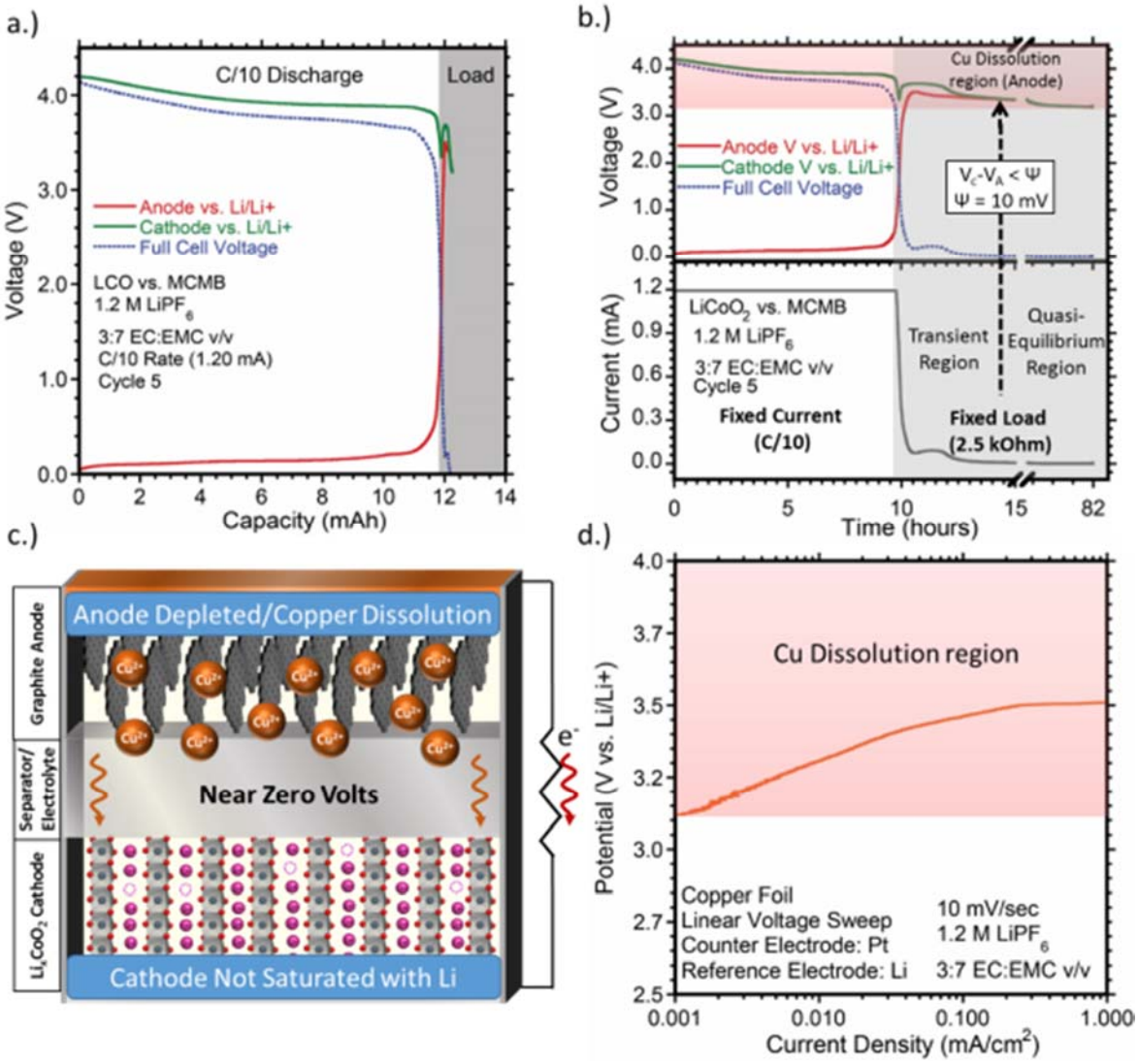

Figure 23. (a) 5th cycle discharge and fixed load step (grey shading) cell voltage and electrode potentials plotted vs. cell capacity, (b) 5th cycle discharge and fixed load step (grey shading) cell voltage and electrode potentials plotted vs. time, (c) Schematic of cell function in the near zero volt condition, (d) Linear sweep voltammogram of copper foil.

Notes: Figure 23 reproduced from reference 17. Red shading represents anode potential range in which copper dissolution occurs.

The adverse effects from copper ions being present in the electrolyte will lead to side reactions with the electrolyte, competitive reduction processes with lithium ions, and copper dendrite formation which can lead to internal shorting. Each of these effects can cause significant damage to the cell and reduce its recharge capacity and performance. *Thus, for cells to be tolerant to near zero volt storage, cell design must be modified or different materials used to avoid the copper dissolution degradation mechanism.*

8.2 Reversible lithium management by anode pre-lithiation of $LiCoO_2$/MCMB lithium ion cells as an alternative approach to near zero volt storage tolerance

It can be expected that anode pre-lithiation prior to cell assembly will increase the amount of reversible lithium in a cell, which should change the behavior of the electrode potentials during near zero volt storage. Hypothetically, a cell having more reversible lithium than necessary to fully lithiate the cathode upon discharge will prevent the anode potential from increasing to the copper dissolution potential upon fixed load discharge to near zero volts. If the amount of pre-lithiation is minimal, damage to the cathode, which can result from a low cathode potential during near zero volt storage, can also be minimized or mitigated. Thus, anode pre-lithiation is a potentially effective approach to realize lithium ion cells that are highly tolerant to near zero volt storage.

Anode pre-lithiation does not introduce unconventional materials or necessitate change in the battery construction parameters, so such an approach can avoid the anticipated trade-offs of the current and past approaches to near zero volt storage tolerance. Additionally, anode pre-lithiation in concept could be applied to a range of difference active material combinations, since there are no operational concerns related to secondary active material stability or reactions with the primary active material.

Pre-lithiation of a graphite anode has also been shown to have the additional benefit of improving performance of conventional cells which can help to reduce the cost/benefit ratio. Also, it may eliminate the need for formation cycling, which could serve to reduce manufacturing costs. Thus, addition of anode pre-lithiation to the battery manufacturing process may not substantially increase the cost of lithium ion cells and could improve general performance in addition to enabling near zero volt storage tolerance.

Additionally, several methods of pre-lithiation with potential for industrial scalability exist. Use of SLMP has been shown to be an effective way to pre-lithiate anodes. Electrochemical pre-lithiation such as bath pre-lithiation has also been developed and is a promising option that is scalable. Therefore, industrially scalable pre-lithiation methods exist and could be utilized for large scale production.

8.2.1 Composite Fabrication and cycling protocols

In the present work, the anode was prepared by mixing MCMB's into a slurry with SuperC™ Carbon Black, SFG-6 and PVDF (Solvay) in a 93:0.3:2.7:4 w/w ratio using NMP as the solvent. The PVDF was dissolved first in the NMP and then the conductive additive and active material was added in succession with intermediate mixing steps. All mixing was done with a Thinky AR-100 planetary mixer. The slurry was coated onto a 20 μm thick copper foil using a doctor blade. The composite was then dried overnight in a vacuum oven at 90 ^{0}C and then calendared to a composite density of ~1.2 g/cm^3. The cathode was prepared by mixing $LiCoO_2$ (MTI Corp) into a slurry with SuperC™ Carbon Black, SFG-6 and PVDF (Solvay) in a 90:5:5 w/w ratio. The mixing procedure was the same as described for the anode using NMP as the solvent. The cathode slurry was coated onto a 20 μm aluminum foil using a doctor blade.

The composite was dried overnight in a vacuum oven at 90 ^{0}C and then calendared to a composite density of ~2.2 g/cm^3.

The cathode is loaded at ~19.3 mg/cm^2 of $LiCoO_2$ giving an areal capacity of ~2.7 mAh/cm^2. The anode is loaded at ~10 mg/cm^2 of MCMB/SFG-6, giving an areal capacity of ~3.0 mAh/cm^2 (conservatively using 300 mAh/g as the capacity of the active material). The area of the electrodes used is 4.5 cm^2, giving a total cathode capacity of ~12.2 mAh and an anode capacity of ~13.5 mAh. The 10% excess of anode capacity compared to the cathode is common practice to reduce the risk of lithium plating on the anode during cycling.

For pouch cells used in the present study, each cycle of experimental cells with a reference electrode utilized a charge step which referenced a cathode potential maximum of 4.2 V vs. Li/Li$^+$. The potential of the cathode vs. Li/Li+ was selected as the control for the upper charge limit to ensure that for all experimental 3-electrode cells in the present study, the cathode is charged to the same degree independent of anode variation. The stability of $LiCoO_2$ is known to be sensitive to the degree which it is charged to, particularly when overcharged. Therefore, utilizing the cathode potential vs. Li/Li$^+$ as the upper charge limit helps eliminate the degree of cathode charge as a variable affecting the cell's cycling performance. Prototype cells and cells constructed for anode pre-lithiation that do not employ a reference electrode utilized a cell voltage of 4.1 V as the upper charge limit, which is a standard charge cutoff voltage for a $LiCoO_2$/MCMB lithium ion cell. All cells were discharged to 3.0 V cell voltage, which is a standard cutoff value for a $LiCoO_2$/MCMB cell.

8.2.2 Electrode Asymptotic Potential

As shown in Figure 24b, after a period of time the electrode potentials asymptote to within a small potential difference of each other and no longer change significantly (cell reaches quasi-equilibrium state). It is therefore convenient to define a single potential that is representative of the minimally varying potential of both electrodes when the cell is in the quasi-equilibrium state. This quantity will be defined herein as the electrode asymptotic potential (EAP) and is described by equation 2 where $\boldsymbol{V_C}$ is the cathode potential vs. Li/Li$^+$ and $\boldsymbol{V_A}$ is the anode potential vs. Li/Li$^+$.

$$\boldsymbol{EAP = \frac{V_C - V_A}{2} + V_A \quad when\ (V_C - V_A) < \Psi} \tag{2}$$

The threshold potential difference Ψ is chosen to represent when the cell reaches a quasi-equilibrium state in which the electrode potentials no longer change significantly. Ψ may have to be defined differently for different cell configurations, fixed load values and active materials used. The value of Ψ is chosen to be 10 mV in the present study. Once the electrode potential difference reaches Ψ, the EAP drifts by only ~0.1 V during the remaining 66 hours of the fixed load period, indicating that 10 mV is a sufficient choice for Ψ in the present case.

8.2.3 Pre-lithiation process and resulting effect on behavior of electrode potentials during normal charge and discharge

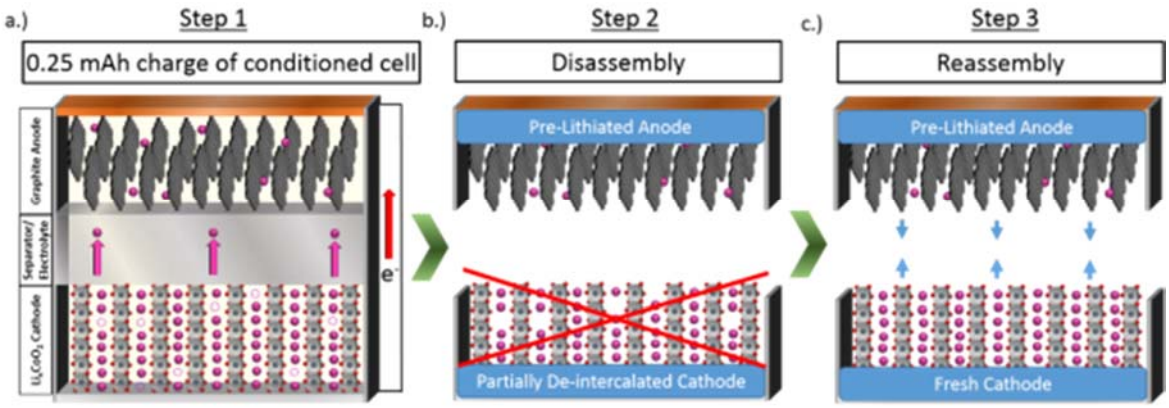

Figure 24. (a) Schematic of 0.25 mAh charge of a conditioned, discharged cell, (b) Schematic depicting disassembly of cell and discarding cathode, (c) Schematic of reassembly for partially lithiated anode with fresh cathode in a new cell.

Note: Figure 24 reproduced from reference 17

In the present work, a lab-scale pre-lithiation method using a sacrificial cathode is used for demonstration of the approach. A $LiCoO_2$/MCMB cell is built with a pre-lithiated anode. Initially, a $LiCoO_2$/MCMB pouch cell was constructed (without a lithium reference electrode) and was cycled at a C/10 rate twice from 3.0-4.1 V cell voltage then partially charged by 0.25 mAh as depicted in Figure 24a. At this state of cycling, the SEI layer on the anode will be formed and the MCMB will be partially (~2% of its capacity) lithiated, whereas the cathode is partially depleted of lithium. The cell was then disassembled and the partially-lithiated anode was reassembled into a cell with a fresh $LiCoO_2$ cathode) which is intrinsically fully lithiated. Since the cathode is fully lithiated, the SEI is already formed on the anode and the anode has some lithium intercalated into it, it can be expected that the resulting cell will have more reversible lithium than is required to fully intercalate the cathode upon discharge. This will be referred to as a RLE cell condition.

The RLE cell with a lithium reference electrode was conditioned by cycling once at a C/20 rate and then four times at a C/10 rate. The cell was charged and discharged between 3.0 V full cell voltage and a cathode potential of 4.2 V vs. Li/Li+. The first cycle charge and discharge curves of the RLE cell, including the electrode potentials as measured by a lithium reference electrode, are shown in Figure 25a and b, respectively. It is observed that the increase of the amount of reversible lithium has changed the behavior of the electrodes during normal charge and discharge. At the start of the charge, the anode potential is ~700 mV vs. Li/Li^+ lower than the conventional cell (i.e. 0.374 V RLE vs. 1.105 V conventional) and as a result the cell voltage is ~700 mV vs. Li/Li^+ higher during the initial stage of charge (i.e. 3.460 V RLE vs. 2.773 V conventional). The lower anode potential at the beginning of charge is consistent with it being partially lithiated upon cell assembly. At the end of charge, it is important to note that since the anode potential is greater than 0 V vs. Li/Li^+ (i.e. ~50 mV), it still has sufficient capacity to

intercalate all lithium during the charge. This indicates that despite pre-lithiation of the anode prior to final cell assembly, no lithium plating is likely to be occurring.

At the end of discharge, the cathode potential is ~350 mV lower in the RLE cell than in the conventional cell (3.360 V RLE vs. 3.789 V conventional). The lower cathode potential at the end of discharge indicates that at this point the cathode is approaching full intercalation. The anode potential is also ~350 mV lower in the RLE cell than in the conventional cell at the end of discharge (0.355 V RLE vs. 0.785 V conventional). The lower anode potential at the end of discharge indicates that at this point the anode is not fully depleted of reversible lithium as depicted Figure 25c. Thus, the process of using a pre-lithiated anode manifests itself in changes to the behavior of the electrode potentials during normal charge and discharge. This is expected to impact the resulting transient behavior of the electrode potentials and the cell's EAP during near zero volt storage under fixed load.

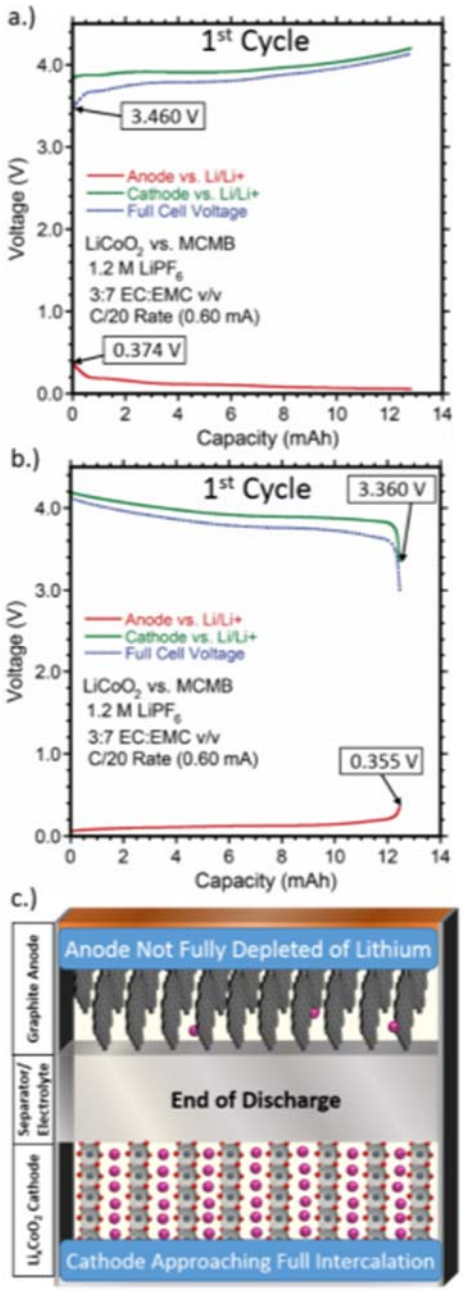

Figure 25. (a) 1st cycle charge cell voltage and electrode potentials of RLE cell (b) 1st cycle discharge cell voltage and electrode potentials of RLE cell, (c) Schematic of cell condition at the end of discharge to a cutoff volt of 3.0 volts showing the cathode fully intercalated and the anode not fully depleted of reversible lithium.

Note: Figure 25 reproduced from reference 17. Labeled voltages represent anode potential and full cell voltage at the beginning of charge

8.2.4 Electrode potential behavior during near zero volt storage of an RLE cell

After the C/10 discharge to 3.0 V cell voltage on the 5th conditioning cycle of the RLE cell, a constant load of 2.5 kOhms was applied to the cell to discharge it to near zero volts (i.e. actual voltage reaches 1-3 mV). The fixed load was applied for three days to represent an extended near zero volt storage period. The 3-electrode data during the 5th cycle discharge is shown as a function of discharge capacity in Figure 26a and as a function of time in Figure 26b. As shown in Figure 26b, during the C/10 discharge (first 10 hours) the cell current is constant and the electrode potentials exhibit their normal discharge behavior. At ~10 hours, the cell reaches 3.0 V and the fixed load (2.5 kOhm) step is initiated. Under fixed load, the RLE cell, undergoes a transient period as it discharges to near zero volts. The cell voltage decreases to <0.1 V in the first two hours which under the fixed load corresponds to a cell current of <0.04 mA. During the first two hours the cathode potential initially decreases to ~1.3 V vs. Li/Li$^+$ and then increases to ~1.4 V vs. Li/Li$^+$. The anode potential initially increases to ~0.6 V vs. Li/Li$^+$, then decreases to ~0.5 V vs. Li/Li$^+$ as the cell current decreases. The anode potential then increases to >1.0 V vs. Li/Li$^+$ after 2 hours at fixed load. After the first 2 hours the potential of both electrodes increases until they asymptote to within 10 mV of each other at ~1.9 V vs. Li/Li$^+$ realizing the EAP for this cell. At this point the cell voltage is <10 mV and the cell current is <4 μA (C/3000) which is considered a quasi-equilibrium state. The quasi-equilibrium state remains for the final 67 hours of the fixed load step. The EAP increases to ~2.0 V vs. Li/Li$^+$ then decreases back to ~1.9 V vs. Li/Li$^+$ during this period.

The initial decrease of the cathode potential below its normal operating potential range without recovery at ultra-low cell currents is attributed to the cathode being fully intercalated with lithium during the overdischarge and possibly undergoing over-insertion. Apparent intercalation of ~0.7 mAh of additional charge into the cathode during the fixed load step may be due to cathode degradation processes since it primarily occurs at <1.636 V vs. Li/Li$^+$, where $LiCoO_2$ has been reported to degrade in an equilibrium condition. The anode potential staying below 2.0 V vs. Li/Li$^+$ during the transient period and the EAP of the cell being ≤2.0 V vs. Li/Li$^+$ indicates that the anode is not fully depleted of intercalated lithium in the near zero volt state of charge. Importantly, the anode potential stays well below ~3.1 V vs. Li/Li$^+$ during the entire fixed load near zero volt storage period. This suggests that the design is stable for such near zero volt storage in that no copper dissolution is expected to be occurring.

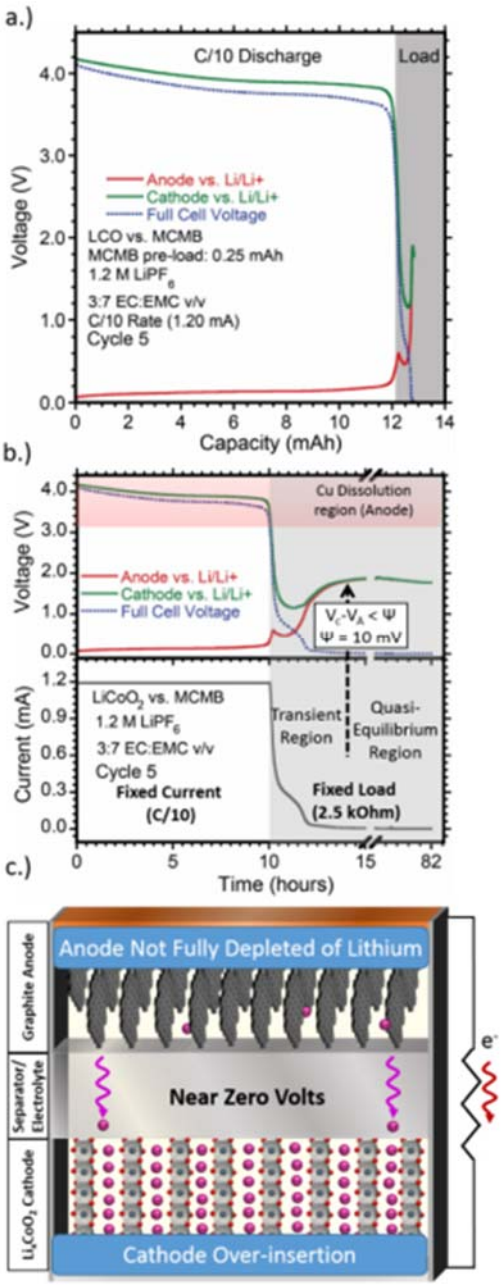

Figure 26. (a) 5th cycle discharge and fixed load step (grey shading) cell voltage and electrode potentials plotted vs. cell capacity of RLE cell, (b) 5th cycle discharge and fixed load step (grey shading) cell voltage and electrode potentials plotted vs. time of RLE cell, (c) Schematic of RLE cell function in the near zero volt condition.

Note: Figure 26 reproduced from reference 17. Red shading represents anode potential range in which copper dissolution occurs. Pink arrows represent lithium ion flow, the red arrow represent electron flow through internal circuit.

8.2.5 Performance retention after near zero volt storage of RLE and conventional cells

The performance retention after near zero volt storage of the RLE cell and the conventional cell was compared using the cycling regime depicted in Figure 27a. After conditioning cycles, a fixed load of 2.5 kOhm was applied to each of the cells for three days to store them at near zero volts. Each cell was then charged at a C/200 rate to 3.0 V cell voltage to gradually bring the cell back to its normal voltage range, as has been done in testing of commercial near zero volt capable cells using a titanium current collector. Then each cell was charged at a C/10 rate to a cathode potential of 4.2 V vs. Li/Li^+ and then discharged at C/10 to 3.0 V cell voltage. Then, the fixed load was again applied and the cycle repeated.

The discharge profiles of the conventional cell before and after intermediate 3-day fixed load, near zero volt storage periods are plotted in Figure 27b. As shown, the conventional cell fades rapidly on cycle 3 to <20% of its original capacity with significant degradation in the discharge voltage characteristics. Both the cathode and anode discharge behavior in the conventional cell was degraded by the near zero volt storage period. The reference electrode measurements show that both electrodes lose all typical discharge characteristics and demonstrate substantial capacity loss. In comparison, Figure 27d shows that the RLE cell exhibits minimal capacity fade by delivering ~99% of its original discharge capacity after the third, 3-day near zero volt storage period. Additionally, only a minor fade in the average discharge voltage of 25 mV was observed. Such a drastic improvement in performance retention over the conventional cell is attributed to the fact that as measured by the reference electrode, the potential of the anode never exceeds 2.0 V vs. Li/Li^+ during each near zero volt storage period. This is well below the assigned copper dissolution potential of 3.1 V vs. Li/Li^+ and as such no copper dissolution is expected to be occurring.

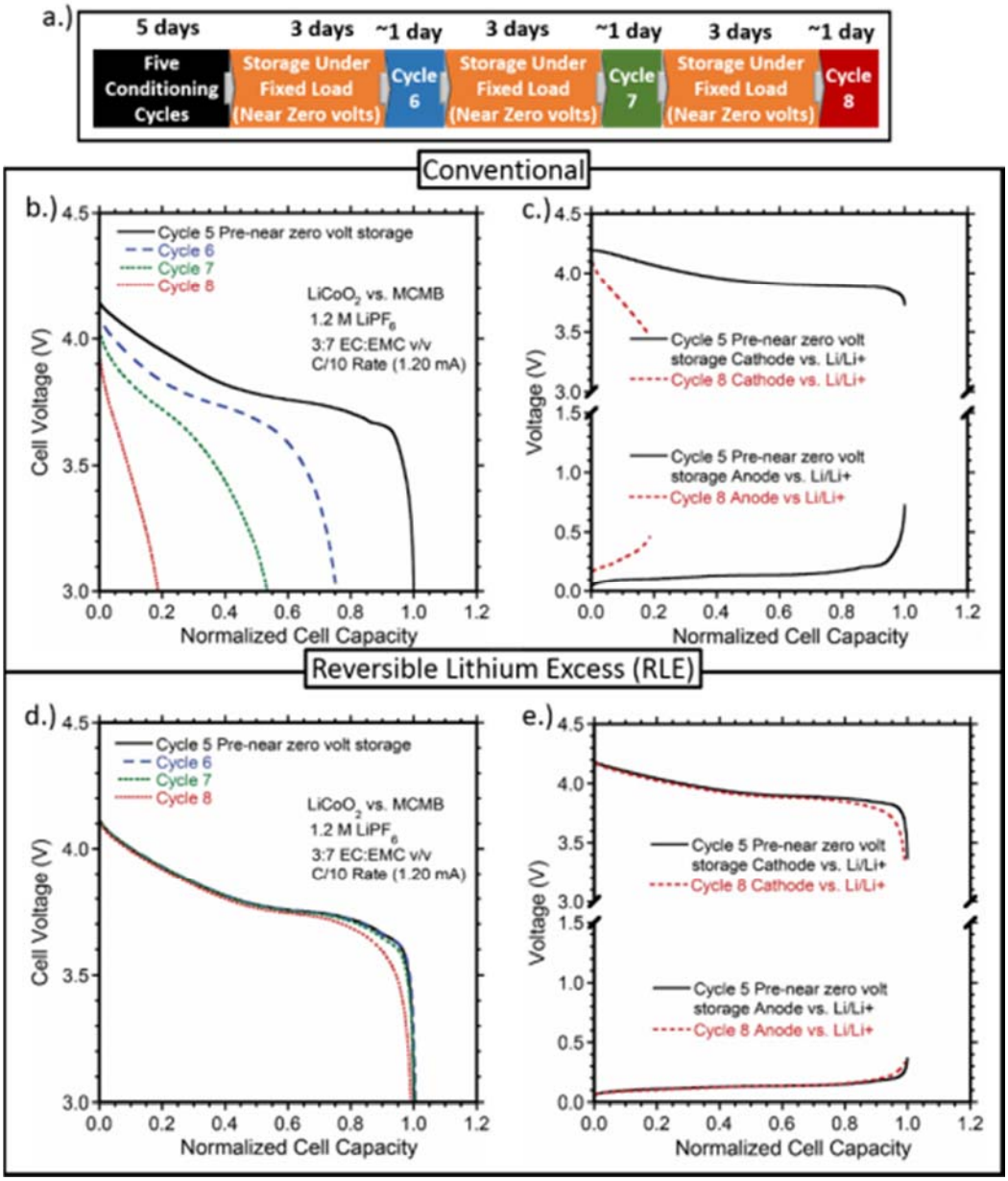

Figure 27. (a) Cycling schedule flow chart, (b) Discharge profiles of a conventional cell prior to zero volt storage and after one, two and three, 3-day near zero volt storage periods, (c) Discharge profile of the conventional cell electrode potentials as measured by a lithium metal reference prior to near zero volt storage and after three, 3-day near zero volt storage periods, (d) Discharge profiles of an RLE cell prior to zero volt storage and after one, two and three, 3-day near zero volt storage periods, (e) Discharge profile of the RLE cell electrode potentials as measured by a lithium metal reference prior to near zero volt storage and after three, 3-day near zero volt storage periods.

Note: Figure 27 reproduced from reference 17

Three-electrode measurements of the RLE cell on the cycle prior to near zero volt storage and after the third, 3-day near zero volt storage period are shown in Figure 27e. During cycle 3, the cathode discharge potential of the RLE cell fades slightly throughout the discharge and at the end of discharge, the potential drop-off is more gradual. The anode discharge potential on the other hand does not notably change at all throughout the majority of the discharge. Only a slight rounding of the potential curve at the end of discharge is observed. Thus, the minor fade of the RLE cell observed is primarily attributed to fade in the cathode discharge performance. Fade in the cathode discharge performance likely results from the cathode potential decreasing to less than the cited degradation potential of 1.636 V vs. Li/Li^+ during the transient period of fixed load storage. However, high performance retention reflects that this damage is minimal and that a cell constructed in the manner of an RLE cell has high tolerance for near zero volt storage conditions.

A second RLE type cell constructed in the same manner was cycled in the same regime but with 7-day fixed-load near zero volt storage periods instead of 3-day periods. The benefit of this test is to further investigate the potential of RLE type cells for longer term storage at near zero volts. The resulting discharge profiles before and after each intermediate storage period are shown in Figure 28**.** As shown, with 99% capacity retention and an average discharge voltage fade of only 16 mV after the third, 7-day storage period at near zero volts, the cell showed nearly identical capacity and discharge voltage retention as the RLE cell stored at near zero volts for 3-day periods. As with the cell stored for 3-day periods, the minor fade of the RLE cell stored at near zero volts for 7-day periods is primarily attributed to fade in the cathode performance as shown in Figure 28c by reference electrode measurements.

The lack of increase in the fade rate of the RLE cell with the increase in storage period time at near zero volts is attributed to the fact that most electrochemical processes occur during the transient period (first ~4-5 hours) of fixed load storage. After that, the cell reaches a quasi-equilibrium state and very little current flows. Thus, it is likely that even longer storage periods will have little to no impact on the fade rate of the cell and that the main factor effecting cell fade rate is the number of times the cell is overdischarged to near zero volts.

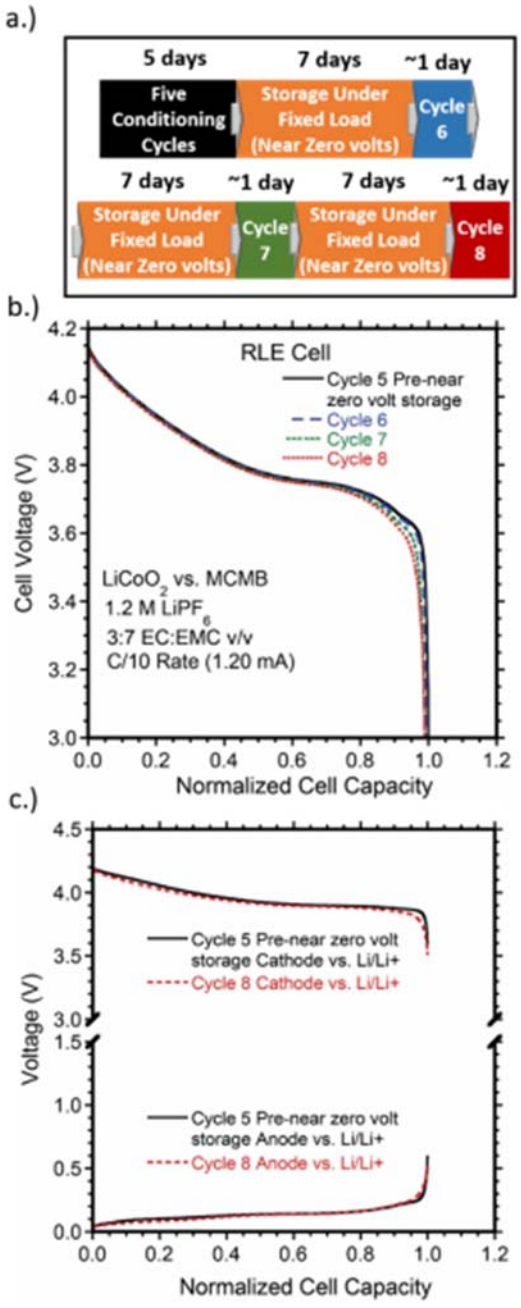

Figure 28. (a) Cycling schedule flow chart, (b) Discharge profiles of an RLE cell prior to near zero volt storage and after 1, 2 and 3 7-day near zero volt storage periods, (c) Discharge profile of the RLE cell electrode potentials as measured by a lithium metal reference prior to near zero volt storage and after 3, 7-day near zero volt storage periods.

Note: Figure reproduced from reference 17

8.2.6 Effect of near zero volt storage on rate capability and long term cycling

Conventional and RLE $LiCoO_2$/MCMB cells were constructed (without reference electrodes). The cycling schedule for the cells is shown in the flow chart in Figure 29a. The cells were cycled between 3.0-4.1 V and conditioned with 1 cycle at a C/20 rate followed by 4 cycles at a C/10 rate. After the 5th cycle discharge the RLE cell was stored at near zero volts with a 2.5 kOhm load applied to the cell for 3 days. The conventional cell on the other hand was stored at open circuit (OC) for 3 days after the 5th cycle discharge.

After the 3-day storage period, the RLE cell was charged to 3.0 V at a C/200 rate, then both the RLE and conventional cells underwent a rate study in which the charge rate was held constant at C/10 and the discharge rate was varied to C/10, C/2, C and 5C as shown in Figure 29b. The data indicates that the rate capability of the RLE cell is nearly identical to the conventional cell, confirming that the 3-day storage period at near zero volts did not have a negative effect on the rate capability of the cell.

After the rate study, the conventional and RLE cells were charged at C/10 and then put on 30% depth of discharge (DOD) LEO cycling. The cycling regime consists of a ~C/2.9 charge to a 4.1 V constant voltage step for 54 minutes followed by a C/2 discharge for 36 minutes. The end of discharge voltages is shown for each cell in c. The RLE cell cycles with the same stability as the conventional cell for 500 cycles, indicating that the 3-day near zero volt storage period had no significant effect on the RLE cell's cycling stability for 31 days of cycling. The benefit of the rate study and LEO cycling is to show that in addition to discharge capacity and voltage retention at a C/10 discharge rate, the discharge rate performance and long-term cycling stability of an RLE cell is not reduced by an extended near zero volt storage period.

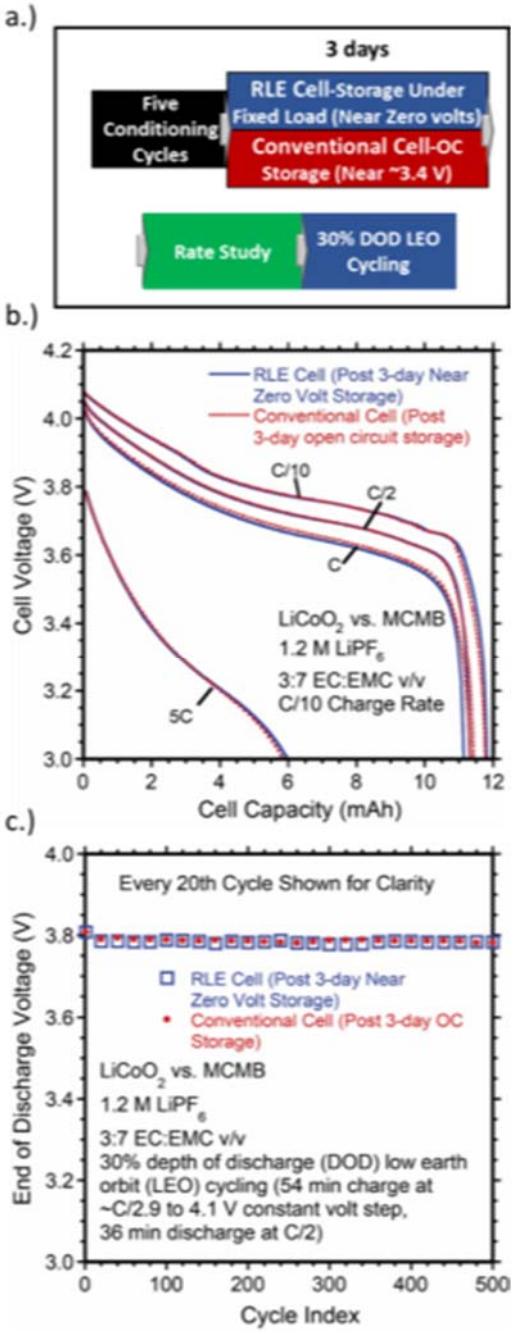

Figure 29. (a) Cycling schedule flow chart showing flow of conditioning, storage, rate testing and LEO cycling. (b) Discharge profiles of RLE and conventional cell at different discharge rates. (c) End of discharge voltages for 30% DOD LEO cycling of the RLE and conventional cell.

Note: Figure 29 reproduced from reference 17. For (d), Rate study done after a 3-day storage period (near zero volt storage for the RLE cell and open circuit storage for the conventional cell)

8.3 Use of high first cycle loss, high energy density lithium rich cathode materials to enable near zero volt storage tolerance

8.3.1 Introduction

Lithium ion batteries have emerged as the premier chemistry for electrochemical energy storage due to their increased energy/power density and tunable performance characteristics compared to other chemistries. Over the last several years, increasing the gravimetric and volumetric energy density of lithium ion batteries has been a primary focus area of research efforts. Batteries with increased energy density can reduce the battery mass required for applications like electric vehicles, home energy storage and other portable applications. However, recent events ranging from automotive and airplane fires, to shipping bans and increased regulations, have highlighted the need to improve the safety characteristics of lithium ion batteries in conjunction with improvements in energy density. It has recently been detailed that if lithium ion cells can tolerate a near zero volt state, batteries can be made safer when they are in a *user-inactive state* (i.e. during storage or transport) by applying a resistor to all individual cells in a battery. In an effectively inert near zero volt state, cells are at substantially reduced risk for thermal runaway, and therefore, are much safer for storage and transport. Additionally, a near zero volt state of charge can rapidly and reliably be confirmed with a handheld voltmeter, meaning a near zero volt shipping requirement would be highly controllable. A more thorough discussion and review of the benefits of near zero volt storage can be found elsewhere.

Conventional lithium ion cells are not tolerant to a near zero volt state of charge, however, and are well known to suffer performance loss if overdischarged due to the anode potential increasing to greater than the copper dissolution potential. To prevent a high anode potential and render advanced cells tolerant to a near zero volt state of charge, an advantageous approach has been to design cells with a precise amount of excess reversible lithium using anode pre-lithiation. However, anode pre-lithiation may have some tradeoffs for manufacturing cost. In this context, an opportunity exists to explore other highly implementable methods to design cells with excess reversible lithium that can tolerate a near zero volt state of charge.

Lithium rich cathode materials exhibit a high first cycle loss which could potentially be used to generate a cell with excess reversible lithium. Lithium rich cathode materials have already generated significant interest in recent years due to their increased energy densities over current state of the art cathode materials. In the present work, the effect of a lithium rich cathode's first cycle loss to maintain the anode potential less than the copper dissolution potential during near zero volt storage under fixed resistive load is investigated. Reference electrode measurements are utilized to investigate the behavior of the electrode potentials of a Li-rich/graphite lithium ion cell during extended near zero volt storage periods under fixed resistive load. The electrode potential behavior during the transient period in which the cell discharges to near zero volts is measured and EAP of the cell is characterized once the cell reaches a quasi-equilibrium, near zero volt state. The recharge performance of the 3-electrode Li-rich/graphite cells after several multi-day near zero volt storage periods is also reported. Conventional 2-electrode pouch cells are tested for the effects of a 3-day near zero volt storage period under fixed resistive load on cell discharge rate capability and longer term cycling stability compared to cells stored at open

circuit. Lastly, elevated temperature testing is also performed to determine the near zero volt storage tolerance of Li-rich/graphite cells at 40°C.

8.3.2 Experimental

Electrode preparation

Cathodes were prepared by mixing TODA America HE5050, which has a structure of $0.49Li_2MnO_3 \cdot 0.51LiNi_{0.37}Co_{0.24}Mn_{0.39}O_2$ into a slurry with SuperC™ Carbon Black, TIMREX® SFG-6 and Solef® PVDF in an 86:2:4:8 mass ratio using NMP as the solvent. The slurry preparation consisted of dissolving PVDF in NMP, followed by mixing in the conductive additives (Carbon Black and SFG-6) and then addition of the HE5050 with intermediate mixing steps. Mixing steps were each performed for 20 minutes using a Thinky AR-100 planetary mixer. The composite slurry was coated onto a 20 μm aluminum foil using a doctor blade. The coated cathode was dried overnight in a vacuum oven at 90°C and then calendared to a composite density of ~1.1 g cm-3. The final active material areal loading was 10.7 mg cm-2 resulting in a first cycle charge areal capacity of 3.26 mAh cm-2 using the measured 305 mAh g-1 first cycle charge capacity at a 0.1225 mA g-1 (~C/20) extraction rate and a discharge areal capacity of ~2.72 mAh cm-2 using the measured 254 mAh g-1 discharge capacity at a 0.1225 mA g-1 (~C/20) insertion rate. The cathode will be referred to as the HE5050 cathode.

Anodes were prepared by mixing Osaka Gas 25-28 MCMB into a slurry with SuperC™ Carbon Black, TIMREX® SFG-6 and Solef® PVDF in a 93:0.3:2.7:4 mass ratio using NMP as the solvent. The slurry preparation consisted of dissolving PVDF in NMP, then by mixing in the conductive additives (Carbon Black and SFG-6) and then addition of the MCMB with intermediate mixing steps in a Thinky AR-100 planetary mixer. The composite slurry was coated onto a 20 μm copper foil using a doctor blade. The electrode was then dried overnight in a vacuum oven at 90°C and calendared to a composite density of 0.985 g cm-3. The final active material areal loading was 11.23 mg cm-2 resulting in a reversible areal capacity of 3.42 mAh cm-2 using the measured 311 mAh g-1 extraction capacity of the graphite (MCMB, SFG-6) in the composite. Using the measured first cycle insertion capacity of 323 mAh g-1 (which includes SEI formation) the first cycle anode insertion areal capacity is 3.63 mAh cm-2. The first cycle insertion anode areal capacity is designed to be at least 10% excess capacity relative to the first cycle charge capacity of the cathode in order for there to be sufficient capacity to accommodate all lithium intercalated into it during the first charge without lithium deposition on the anode. The anode will be referred to as the MCMB anode.

Electrochemical testing

Cells incorporating reference electrodes were constructed using single layer pouch type cells with electrodes of 4.5 cm^2 and the cells were rated at 12 mAh capacity. The cathode and anode were stacked with a Celgard™ separator between them and a 1.2 M $LiPF_6$ 3:7 ethylene carbonate:ethyl methyl carbonate v/v was injected before final sealing of the pouch cell. In the case of pouch cells with a reference electrode, a lithium chip pressed into a copper mesh with an ultrasonically bonded copper tab was placed to the side of the cathode/anode stack on both sides of the separator. A schematic of the pouch cell setup can be found in a previous study.

In the case of coin cells with a reference electrode, a copper tap was inserted around the gasket that seals the cell with Kapton film on both sides of the tab to electrically isolate it from the lid of the coin cell as shown in Figure 30. A lithium chip was then pressed onto the copper before construction of the coin cell. The coin cell was assembled in the order anode->separator>cathode>spacer>wave spring>case (left to right in Figure 30), all while ensuring that the lithium and copper did not physically contact the coin cell case or electrodes. Lithium chip incorporation, electrolyte injection and final pouch cell sealing/coin cell crimping was done in an Argon glove box maintained at <1 ppm oxygen and <1 ppm water.

Figure 30. Coin cells with reference electrode (assembly order left to right)

Pouch cells were cycled using an Arbin BT-2000 cycler outfitted with auxiliary voltage measurements. The cell voltage, cathode potential and anode potential were all monitored independently during cycling of 3-electrode cells. Cells utilizing a lithium reference electrode were cycled galvanostatically to a cathode potential of 4.6 V vs. Li/Li^+ and discharged to a full cell voltage of 2.0 V. Utilizing the cathode potential as the charge cutoff point ensures that the cathode is fully utilized but not overcharged. Conventional 2-electrode were cycled between 2.0 and 4.5 V cell voltage. All tests referred to as 3-days in duration constitute a 72-hour period and all tests referred to as 7-days in duration constitute a 168-hour period. All electrochemical tests were performed at room temperature (~21 °C).

The lithium metal reference electrode used in the present work allows for monitoring of the electrochemical potentials of both the cathode and the anode vs. the Li/Li^+ redox couple during cycling. The present setup is suitable for DC voltage measurements since the measured impedance between the reference electrode and either electrode is ≤10.0 kOhm. The Arbin cycler used in the present study uses a ~10 GOhm impedance for DC voltage measurements, which would result in a sufficiently low measurement error of ≤1.0 μV caused by the IR drop in the fabricated cell. Additionally, the difference of the measured cathode potential and anode potential deviates by <8 mV from the measured cell voltage throughout all cycling in the present work, indicating the setup is valid.

8.3.3 Results and discussion

First Cycle charge and discharge

It is well documented that many lithium rich layered cathode materials have a high irreversible capacity loss during the first charge/discharge cycle of ~20%. In the case of the material used in the present study, the first cycle loss is measured to be 19.7%. In comparison, the graphitic anode exhibits a first cycle loss of about 5% due to SEI formation. In full cells, the cathode and anode must be capacity matched so that the anode has sufficient capacity to manage

all lithium extracted from the cathode on the first cycle charge to avoid lithium deposition. In the present work, the first cycle anode insertion areal capacity (which includes SEI formation and intercalation capacity) is designed to be about 10% excess of the cathode's first cycle charge capacity. The first charge of the HE5050/MCMB cell shown in Figure 31a requires 13.52 mAh of charge capacity to charge until the cathode reaches 4.6 V vs. Li/Li^+. As shown in Figure 31a, at the end of the first cycle charge, the anode electrochemical potential is 28 mV vs. Li/Li^+, indicating it is not fully intercalated with lithium and confirms the designed excess capacity. Figure 31b shows the first discharge, which delivers 11.3 mAh at the cutoff cell voltage of 2.0 V.

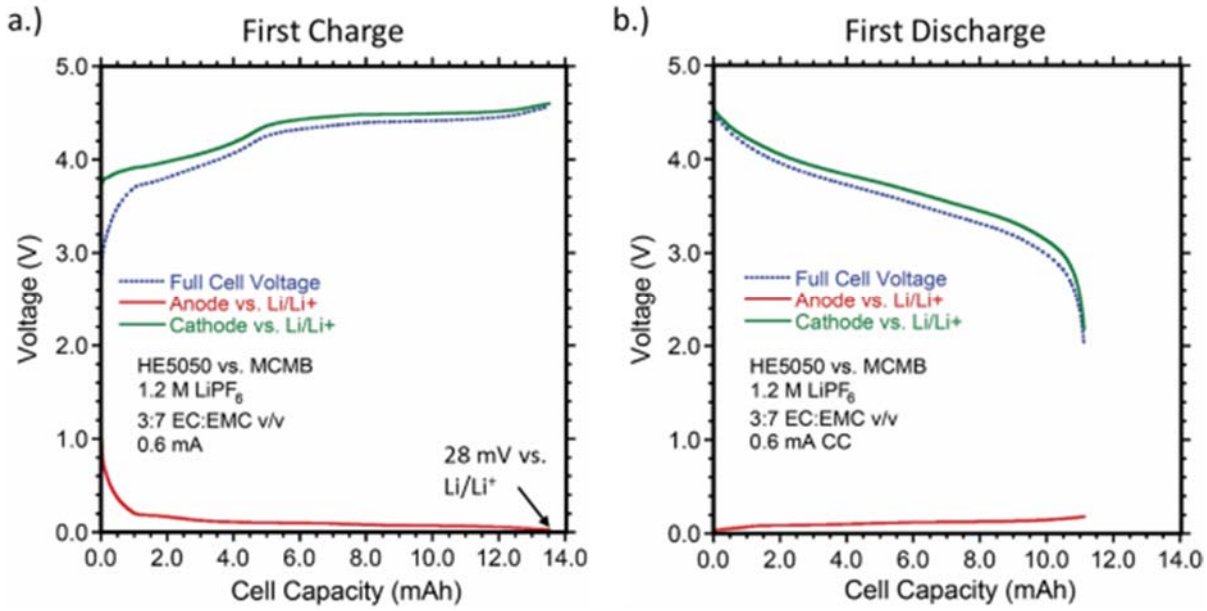

Figure 31. (a) Electrode potentials and cell voltage during first charge with a constant current (CC) of 0.6 mA. (b) Electrode potentials and cell voltage during the first discharge with CC of 0.6 mA.

Note: Figure 31 reproduced from reference 18

At the end of discharge, the anode potential remains in its normal 100-200 mV vs. Li/Li^+ range indicating the anode still contains reversible lithium at the end of discharge. The insertion transformations of the cathode that occur between the resulting cathode discharge range of 2.1-4.6 V vs. Li/Li^+ are fully saturated as evidenced by the cathode potential decreasing rapidly at the end of discharge.

Using a series of calculations, the amount of reversible lithium in the cell can be tracked throughout cycling based on the charge/discharge capacities of the cell and the amount of lithium consumed by SEI formation on the anode as measured in half-cells. Specifically, after each charge, the amount of lithium consumed by SEI on the anode, as measured by half-cell data, is subtracted from the amount of lithium inserted into the anode on charge (i.e. the cell's charge capacity) to yield the amount of reversible lithium in the anode after charge. Then, from this calculated amount of reversible lithium in the anode, the amount of lithium extracted from the anode on discharge (i.e. the cell's discharge capacity) is subtracted. The amount of reversible

lithium in the anode after discharge of the cell to 2.0 V will be referred to as the amount of excess reversible lithium in the cell. The amount of excess reversible lithium calculated to remain in the anode after the first cycle discharge is 1.85 mAh.

8.3.4 Electrode behavior during fixed resistive load near zero volt storage

Experimental 3-electrode cells were conditioned for 4 additional cycles at a 1.2 mA charge/discharge current (i.e. C/10 based on rated cell capacity) after the first cycle. Following the 5th cycle discharge to 2.0 V, a fixed resistive load of 1.67 kOhm was applied for 72 hours to simulate a resistor being applied across the leads of a battery. A fixed resistive load is selected as a controlled method to decrease the cell potential to a near zero volt state, as it represents a highly implemental approach for practical storage of cells in the field. The load value in the present work was designed to give a 1.2 mA current rate when the cell voltage is at 2.0 V Figure 32a shows the cell voltage and electrode potentials during the 5th cycle discharge and fixed resistive load step plotted as a function of cell capacity. Figure 32b shows the cell potential and electrode potentials during the 5th cycle discharge and fixed resistive load step plotted as a function of time.

As shown in Figure 32b, after the 5th constant current discharge and application of the fixed resistive load, the cell undergoes a transient period in which the cell potential decreases to near zero volts. During the transient period, the potential of the cathode initially decreases to ~1.5 V vs. Li/Li$^+$ where it plateaus for the first few hours. The cathode insertion plateau at ~1.5 V vs. Li/Li$^+$ is an expected feature of layered lithium rich cathode materials.

The anode potential, on the other hand, remains in its normal range of <300 mV vs. Li/Li$^+$ for the same first few hours of the transient period. An additional 2.29 mAh of discharge capacity is realized during this time of the transient period with the cell voltage plateauing at ~1.3 V. The amount of additional discharge is in reasonably close agreement (~7% difference) to the calculated amount of excess reversible lithium stored in the anode of 2.11 mAh). The excess reversible lithium is not extracted during the normal discharge and is only extracted when the cell is overdischarged by an applied fixed resistive load. The slight larger observed amount of excess reversible lithium compared to the calculated amount may be accounted for by the fact that half-cell tests only extracted lithium to 1.5 V vs. Li/Li$^+$, not 2.8 V vs. Li/Li$^+$, which is where the anode potential increased to during near zero volt storage. Additionally, the half-cell's were cycled at a constant current of C/20 and C/10, whereas in the full cell during the fixed resistive load step, the current decreases to a much lower value which can be expected to lead to extraction of more reversible lithium from the anode.

After the first 3 hours of the transient period, the anode potential increases significantly and approaches the cathode potential at ~1.5 V vs. Li/Li$^+$. Figure 32b shows that after the anode reaches ~1.5 V vs. Li/Li$^+$, the potentials of the electrodes vs. Li/Li$^+$ both begin to increase. About 10 hours after the fixed resistive load is applied, the electrode potentials asymptote at ~2.8 V vs. Li/Li$^+$, where they remain for the duration of the fixed resistive load step. At this point, the cell current is <6 μA (~C/2000) and the cell can be considered to be in a quasi-equilibrium state. Despite being in a quasi-equilibrium state, the resistor must remain on the cell, otherwise under an open-circuit condition the cell voltage will recover. Thus, the resistor is required in a realistic

scenario in order to keep the cell voltage constant at a near zero volt, safe state, to be easily read by a voltmeter.

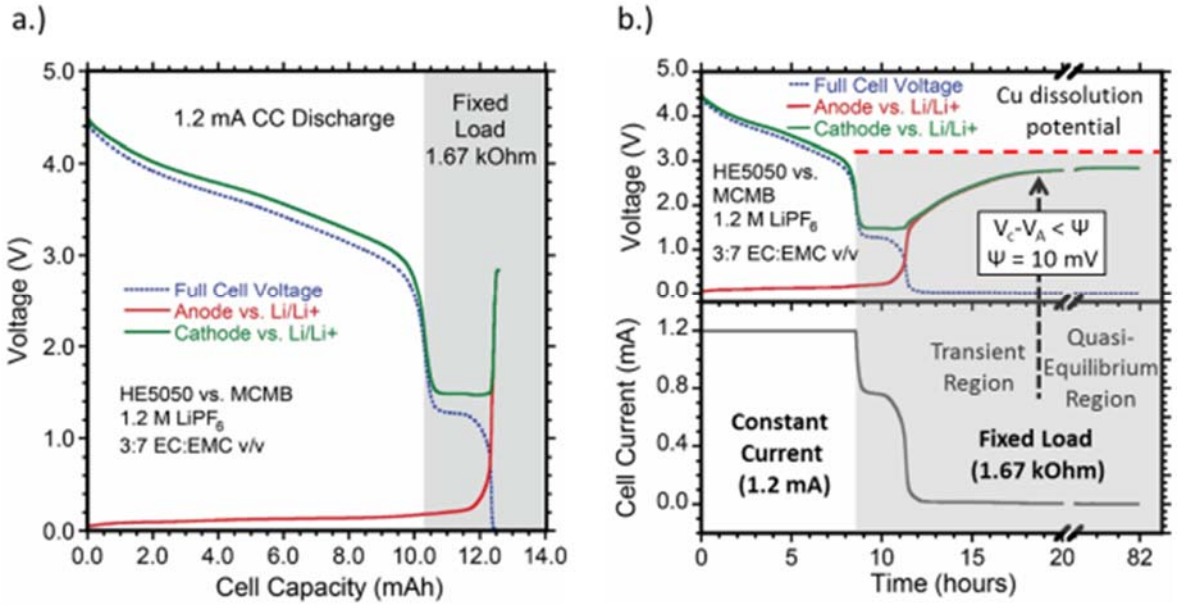

Figure 32. (a) Electrode potentials and cell voltage during 5th 1.2 mA constant current (CC) discharge and 3-day fixed resistive load storage plotted against cell capacity. (b) Electrode potentials and cell voltage during 5th 1.2 mA CC discharge and 3-day fixed resistive load storage plotted against time.

Note: Figure 32 reproduced from reference 18. For (b), the red dashed line represents the electrochemical potential for copper dissolution.

As detailed previously, it is useful to define an EAP that is representative of the semi-constant potential of both electrodes when the cell is in a quasi-equilibrium, near zero volt state under fixed resistive load. Since the electrode potentials remain fairly constant at ~2.8 V vs. Li/Li^+ once the cell voltage decreases to less than 10 mV, Ψ = 10 mV is a sufficient threshold for defining the EAP of the HE5050/MCMB cell. Importantly, the transient period anode potential and EAP of the cell are below 3.1 V vs. Li/Li^+, which is the potential assigned in a previous study at which dissolution of the copper current collector initiates at room temperature. As such, damaging copper dissolution is not expected to be occurring in the HE5050/MCMB cell at room temperature during near zero volt storage. The changes in electrode and cell voltages during fixed resistive load testing highlight the importance of reference electrode measurements. The measured increase in the HE5050 and MCMB electrode potentials after the 1.5 V vs. Li/Li+ intercalation plateau of the cathode and depletion of the anode results in an EAP of ~2.8 V vs. Li/Li^+. Predictions based on capacity matching and extrapolation of fixed current half-cell discharge curves of the individual electrodes would not predict the EAP value in the quasi-equilibrium regime. In comparison, the transient behavior and EAP of previously reported $LiCoO_2$/MCMB cells, with or without anode pre-lithiation, are different for an HE5050/MCMB cell. Thus, the quasi-equilibrium state represents a condition where the cell voltage decreases to <10 mV (with a very low current equivalent to less than C/2000), and the electrode and

electrolyte kinetics are no longer influencing the potentials, rather the thermodynamics of the system dominate. The implication of these results is that the active material chosen for the cathode and the amount of reversible lithium of the cell has an effect on the transient behavior and cell EAP. Overall, the benefits of reference electrode measurements in determining the behavior of the electrode potentials during fixed resistive load, near zero volt storage of a lithium ion cell motivate their utility and necessity for future studies.

8.3.5 Discharge Performance retention after repeated periods of near zero volt storage

The performance retention of the 3-electrode pouch cell after repeated storage periods at near zero volts was tested according to the testing regime described in Figure 33a. After cell conditioning and first application of a fixed resistive load, the cell was recharged with a constant current of 0.06 mA (~C/200) until the cell voltage reached 2.0 V to bring the cell back into its normal voltage range. A very gradual initial charge after near zero volt storage is done presently to ensure testing is similar to what has been done previously for testing of commercial near zero volt capable cells and in previous near zero volt storage studies. After charging the cell to 2.0 V, it was charged with a constant current of 1.2 mA to 4.6 V vs. Li/Li^+ cathode potential and discharged with a 1.2 mA constant current to 2.0 V cell voltage. After discharge, a 1.67 kOhm load was again applied and the cycle repeated. Figure 33b shows the discharge curves for the cycle before near zero volt storage and the cycles after one to five 3-day near zero volt storage periods (NZVSP). The cell maintains >98% of its original capacity with only a 22 mV fade in the average discharge voltage after five, 3-day near zero volt storage periods. The performance retention is primarily attributed to the cell's EAP remaining at ~2.8 V vs. Li/Li^+ for all near zero volt storage periods, which is less than the copper dissolution potential assigned.

The measured discharge performance retention shown in Figure 33b also indicates that the low voltage insertion of the cathode near 1.5 V vs. Li/Li^+ does not significantly degrade the cathode performance. Furthermore, the near zero volt storage coulombic efficiency (NZVSCE) of the cell (calculated by equation 3 where C_{pnzv} is the charge capacity post near zero volt storage, D_{cc} is the discharge capacity of the constant current step, and D_{frl} is the discharge capacity of the fixed resistive load step) of the cell is >99%. The NZVSCE value remains essentially constant (>98%) for all subsequent near zero volt storage periods. Thus, charge passed during the fixed resistive load discharge to near zero volts is highly reversible. Overall, observed discharge performance retention demonstrates that high tolerance to repeated near zero volt storage is attainable with an HE5050/MCMB cell.

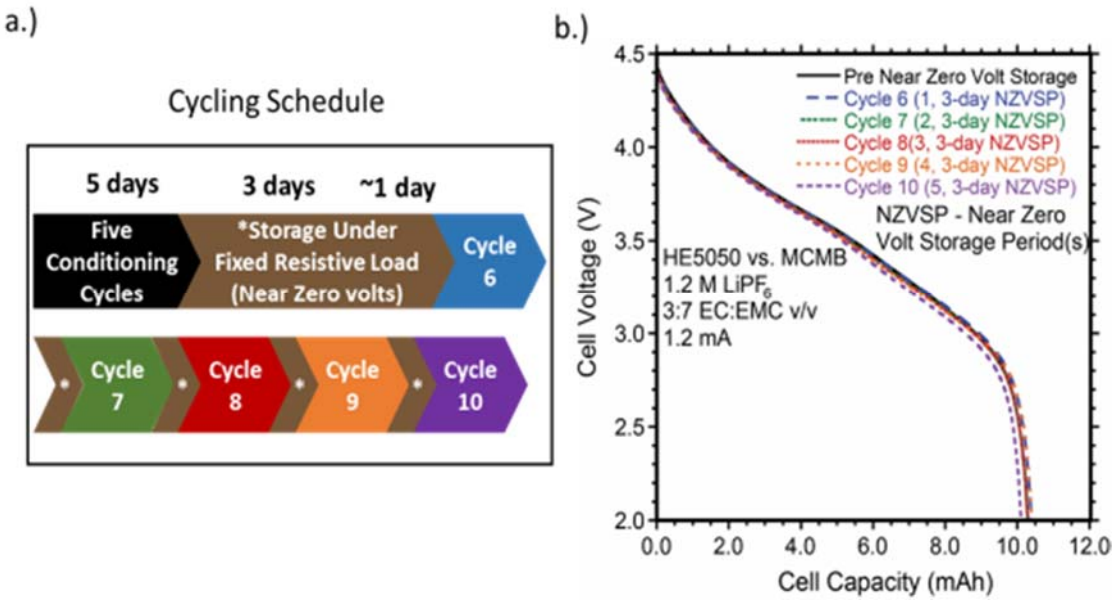

Figure 33. (a) Flowchart of cycling regime for testing the tolerance of the HE5050/MCMB cell to 3 days near zero volt storage periods, (b) 1.2 mA CC discharge curves of HE5050/MCMB cell prior to and after 1, 2, 3, 4, and 5 seventy-two hour, near zero volt storage periods.

Note: Figure 33 reproduced from reference 18

$$NZVSCE(\%) = \frac{C_{pnzv}}{D_{cc}+D_{frl}} \times 100 \quad (3)$$

A second 3-electrode pouch cell was tested in the same manner but with 7-day near zero volt storage periods instead of 3-day storage periods. The benefit of this test is to determine if longer storage periods at the beginning of cell life lead to changes in the discharge performance retention of the cell for this chemistry. The EAP of the cell, as with the cell stored for 3-day fixed resistive load periods, remains at ~2.8 V vs. Li/Li^+ for each near zero volt storage period, so even with longer storage periods at near zero volts, no copper dissolution is expected to be occurring. Additionally, the NZVSCE for each 7-day fixed resistive load storage period is >97%, which is very similar to >98% observed during 3-day near zero volt storage periods. Thus, increasing the time of the near zero volt storage periods does not significantly decrease the reversibility of charge passed during the fixed resistive load, near zero volt storage period.

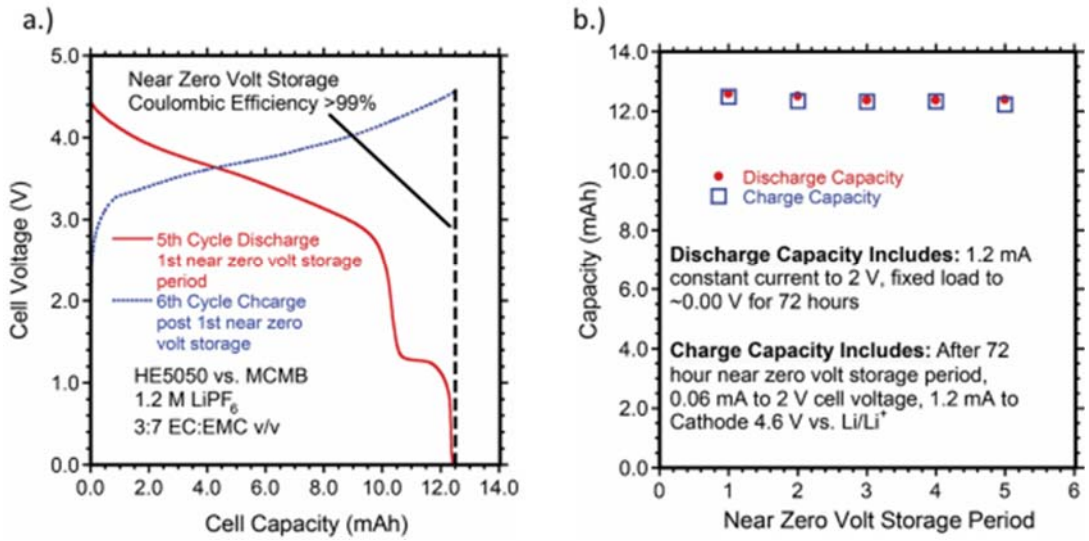

Figure 34. (a) HE5050/MCMB cell voltage profile during the 5th cycle discharge and first 3-day near zero volt storage period under fixed resistive load (solid red line) and the cell voltage profile during the charge following (dotted blue line), (b) Discharge capacity plotted with the charge capacity of the cell charge on subsequent cycle after the near zero volt storage period.

Note: Figure 34 reproduced from reference 18. For (a), Dashed line indicates discharge/charge capacity of each step

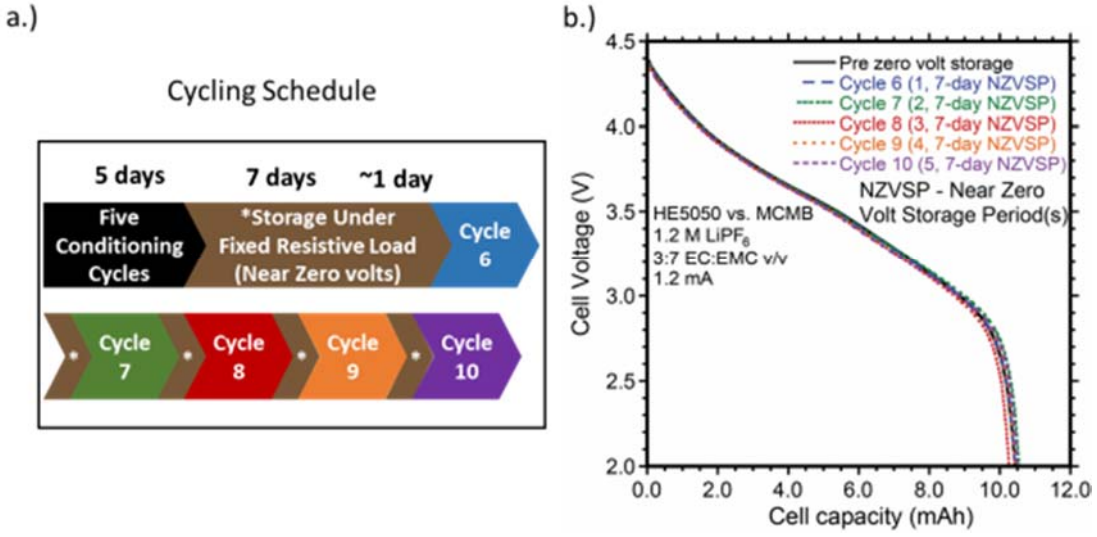

Figure 35. (a) Flowchart of cycling regime for HE5050/MCMB cell at 7 day near zero volt storage periods, (b) 1.2 mA CC discharge curves of HE5050/MCMB cell prior to and after 1, 2, 3, 4, and 5 seven day, near zero volt storage periods.

Note: Figure 35 reproduced from reference 18

As shown in Figure 35b, the cell maintains nearly 100% of its discharge capacity with only a 16 mV average discharge voltage fade after 5, 7-day near zero volt storage periods (35 total days of near zero volt storage). Overall, the results suggest that increased storage time of the cell under fixed resistive load does not increase the fade of HE5050/MCMB cells. The high tolerance can be attributed to an EAP sufficiently less than the copper dissolution potential and high reversibility of charge passed during the fixed resistive load, near zero volt step even with the longer storage periods. Similar to prior study of $LiCoO_2$/MCMB cells which utilized a pre-lithiated anode, the dominant electrochemical reactions take place during the transient period of ~10 hours of fixed resistive load storage, and after that, the cell can be considered to be in a quasi-equilibrium state. Collectively, the results suggest that longer storage periods in conditioned cells are not likely to increase the fade rate of discharge performance in the cells after near zero volt storage.

8.3.6 Effects of near zero volt storage on cell rate capability and long term cycling

Two conventional, 2-electrode HE5050/MCMB pouch cells were constructed and tested according to the flowchart shown in Figure 36a. Cells were cycled for 5 conditioning cycles (one at 0.6 mA constant current and 4 cycles at 1.2 mA constant current) from 2.0-4.5 V cell voltage. After the 5^{th} cycle discharge, one cell was stored at open circuit for 3 days while the other cell was stored at near zero volts under fixed resistive load for 3 days. After the 3-day period, the cell stored at near zero volts was recharged to 2.0 V cell voltage at a 0.06 mA (~C/200) constant current. Then, both cells were analyzed by a rate study in which the charge rate was held constant at 1.2 mA and the discharge rate was varied from 1.2 mA, 6.0 mA, 12 mA and 60 mA (i.e. C/10, C/2, 1C and 5C rates based on rated cell capacity of 12 mAh). The benefit of the rate test is to determine if the cell stored at near zero volts for 3-days has equivalent discharge rate capability compared to the cell stored at open circuit, which would indicate the near zero volt storage period is not detrimental to performance. As shown in Figure 36b, the cell stored at open circuit for 3 days and the cell stored at near zero volts for 3 days had very similar discharge profiles for all tested discharge rates. An increase in capacity retention of about 10% is observed in Figure 36b for the cell stored at near zero volts for 3 days at 1C and 5C rates. Thus, near zero volt storage does not have a negative effect on the rate capability of HE5050/ MCMB cells, and was even observed to lead to minor improvements at discharge rates ≥ 1C.

Following the rate study, each of the conventional HE5050/MCMB 2-electrode cells were cycled using a standard 30% DOD LEO cycling regime, which involves a 54-minute charge (~C/3 charge to a 4.5 V constant voltage step) followed by a C/2 discharge for 36 minutes. The LEO cycling regime was selected because it represents a rigorous, demanding cycling schedule that will be sensitive to any degradation caused by the near zero volt storage. The benefit of LEO cycling is to determine if the cell stored at near zero volts for 3-days has decreased long term cycling stability compared to the cell stored at open circuit, which would indicate the near zero volt storage period is detrimental to the longevity of the cell.

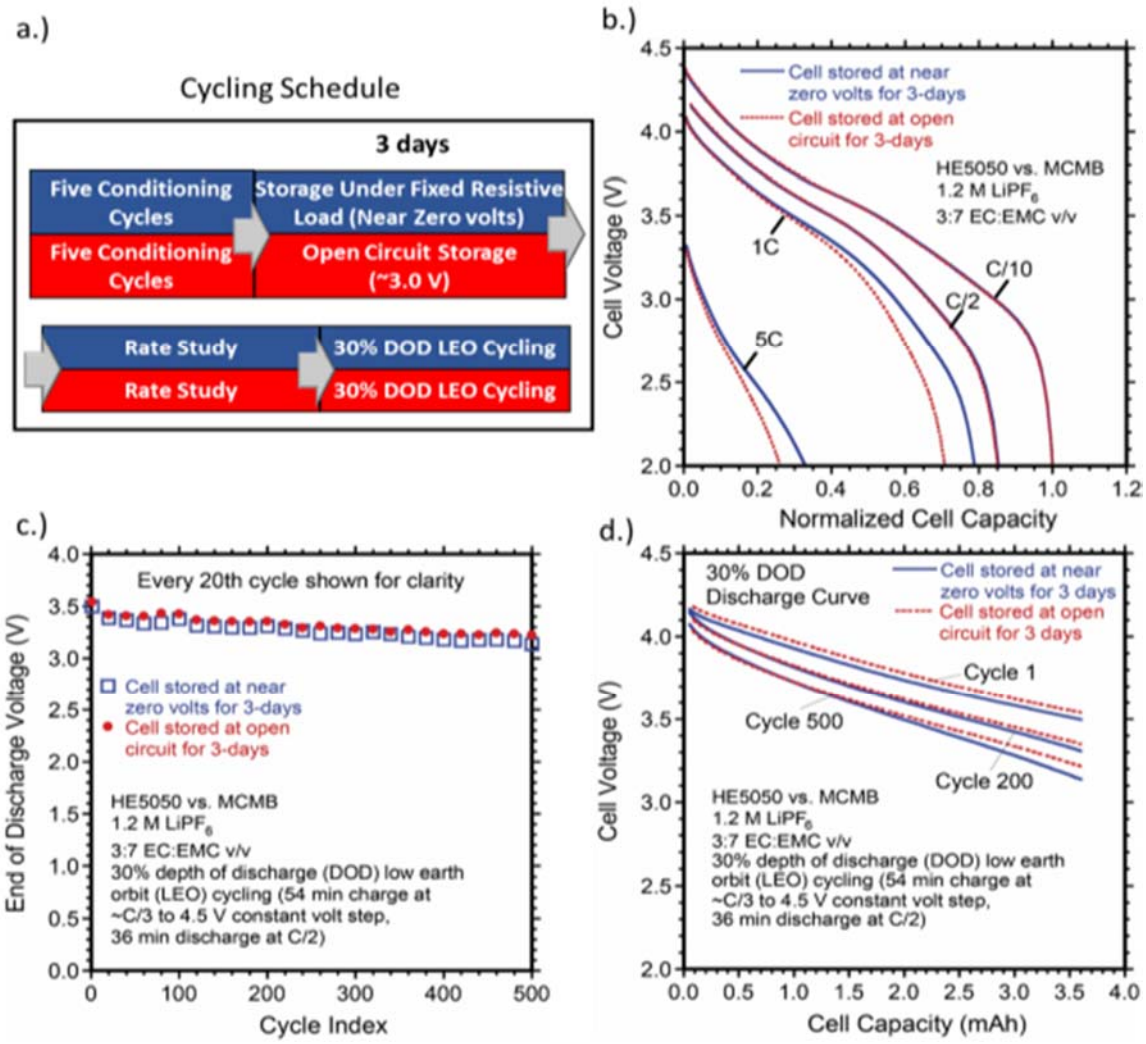

Figure 36. (a) Flow chart of cycling schedule for HE5050/MCMB cells, (b) Discharge profiles of HE5050/MCMB cell stored at open circuit for three days and HE5050/MCMB cell stored at near zero volts for three days at C/10, C/2, C and 5C discharge rates, (c) End of discharge voltages under 30% DOD LEO cycling for HE5050/MCMB cells stored at open circuit for three days and stored at near zero volts for three days, (d) Discharge voltage profile of the 1st, 200th and 500th LEO cycles from (c).

Note: Figure 36 reproduced from reference 18

Figure 36c shows the end of discharge cell voltages for each cycle up to 500 cycles (~1 month of cycling). As observed, the end of discharge voltages are very similar throughout cycling between the cell stored at near zero volts for 3 days and the cell stored in a discharged state at open circuit for 3 days. Figure 36d shows the discharge profiles of the 1st, 200th and 500th cycles, which only display subtle voltage differences. Thus, the 3 days near zero volt storage period at the beginning of life had minimal to no negative effect on longer term cycling stability of the HE5050/MCMB cell. The modest fade observed in both cells is attributed to fade of the HE5050 discharge performance, which is commonly observed in lithium rich cathode materials.

9 CONCLUSIONS

9.1 Cycling Under GEO/MEO

A 3-interface, 4 mAh/cm^2 NCA:MCMB pouch cell was fabricated and conditioned in the RIT Battery Prototyping Center using a 1.2 M $LIPF_6$ EC:EMC (3:7 wt/wt) electrolyte from 4.3V to 2.5V (Figure 37). Upon conditioning, the pouch cell achieved a total capacity of 166.84 mAh at a discharge rate of C/10. After conditioning, the pouch cell was placed on a GEO to 60% DOD using a C/20 charge for 23 hours and a C/2 discharge for 72 minutes. The first GEO cycle reached an end of discharge voltage (EODV) of 3.50V, after which, this pouch cell was allowed to continuously cycle. After 765 cycles, this cell has reached an EODV of 3.31V, retaining 96% of its initial end of discharge voltage. This pouch cell will continue to cycle until reaching an EODV of 2.5V.

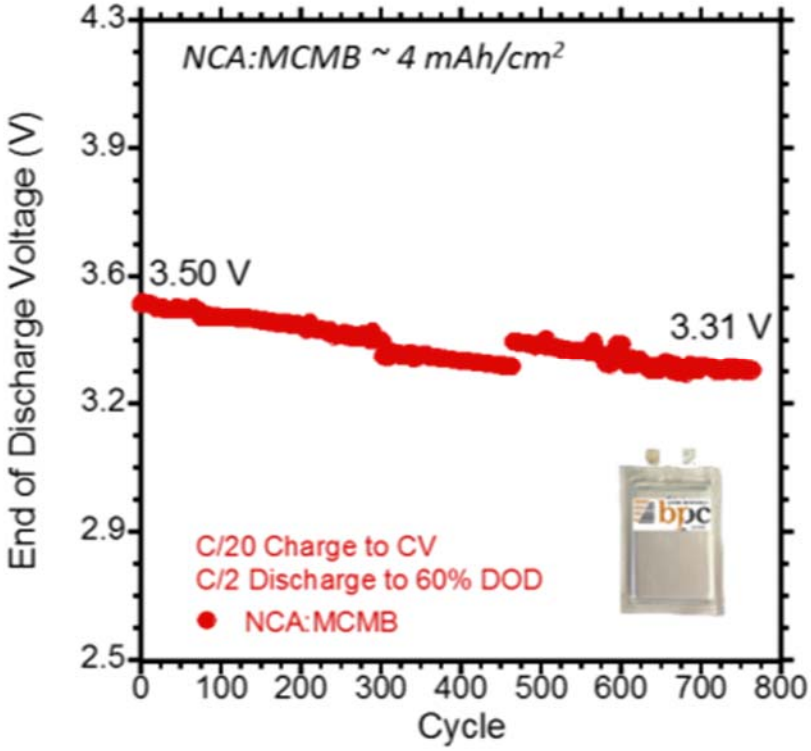

Figure 37. End of discharge voltage for a standard NCA:MCMB pouch cell built in the RIT Battery Prototyping Center at 4 mAh/cm2 loading and cycling under a GEO orbit cycle

9.2 Route to a 400 Wh/kg Zero-Volt Cell

Two pouch cell chemistries, state of the art NCA:MCMB and a lithium rich HE5050:Ge-NP, have been evaluated in an effort to reach 400 Wh/kg. The energy density (Wh/kg) and volumetric energy density (Wh/L) was calculated considering each pouch cell would consist of 32 anodes and 32 cathodes. Two areal capacities (mAh/cm^2) were used in these calculations, a 4 mAh/cm^2 coating, which is a standard areal capacity in the lithium ion battery industry, and a 10 mAh/cm^2 coating. Initial pouch cells have been fabricated using ~20 µm thick copper foil, ~ 20 µm thick aluminum foil and a 25 µm thick Celgard 2520 separator. The potential for increased energy density was calculated by using thinner current collectors and separator material. The potential for higher energy densities using a NCA:MCMB pouch cell reaches its limit prior to 300 Wh/kg, however, a pouch cell using the lithium rich HE5050:Ge-NP electrodes may exceed 400 Wh/kg using an areal capacity of 10 mAh/cm^2.

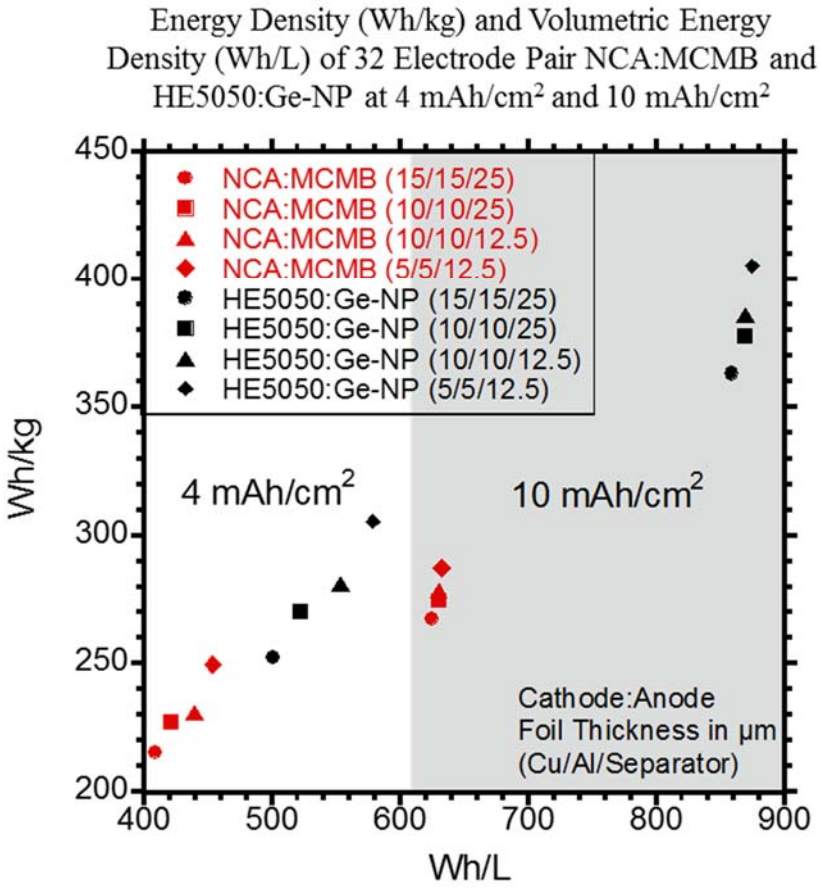

Figure 38. Gravimetric vs. volumetric energy density for high energy cathode and anode designs

REFERENCES

[1] B. Scrosati, "Recent advances in lithium ion battery materials," *Electrochimica Acta,* vol. 45, pp. 2461-2466, 2000.

[2] R. A. DiLeo, *et al.*, "Balanced Approach to Safety of High Capacity Silicon-Germanium-Carbon Nanotube Free-Standing Lithium Ion Battery Anodes," *Nano Energy,* vol. 2, issue 2, pp. 268-275, March 2013.

[3] M. W. Forney, *et al.*, "High performance silicon free-standing anodes fabricated by low-pressure and plasma-enhanced chemical vapor deposition onto carbon nanotube electrodes," *Journal of Power Sources,* vol. 228, pp. 270-280, 2013.

[4] M. W. Forney, *et al*., "Prelithiation of Silicon–Carbon Nanotube Anodes for Lithium Ion Batteries by Stabilized Lithium Metal Powder (SLMP)," *Nano Letters,* vol. 13, pp. 4158-4163, 2013.

[5] M. J. Ganter, *et al.,* "Differential scanning calorimetry analysis of an enhanced LiNi0.8Co0.2O2 cathode with single wall carbon nanotube conductive additives," *Electrochimica Acta,* vol. 56, pp. 7272-7277, 2011.

[6] P. Arora, *et al*., "Capacity fade mechanisms and side reactions in lithium-ion batteries," *Journal of the Electrochemical Society,* vol. 145, pp. 3647-3667, Oct 1998.

[7] C. X. Peng, *et al.*, "Electrochemical behavior of copper current collector in imidazolium-based ionic liquid electrolytes," *Journal of Applied Electrochemistry,* vol. 40, pp. 653-662, Mar 2010.

[8] J. Shu, *et al.*, "Comparative study on surface behaviors of copper current collector in electrolyte for lithium-ion batteries," *Electrochimica Acta,* vol. 56, pp. 3006-3014, Mar 2011.

[9] M. M. Xu and H. D. Dewald, "Impedance studies of copper foil and graphite-coated copper foil electrodes in lithium-ion battery electrolyte," *Electrochimica Acta,* vol. 50, pp. 5473-5478, Sep 2005.

[10] M. C. Zhao, *et al.,* "Electrochemical stability of graphite-coated copper in lithium-ion battery electrolytes," *Journal of the Electrochemical Society,* vol. 147, pp. 3983-3988, Nov 2000.

[11] M. C. Zhao, *et al.*, "Electrochemical stability of copper in lithium-ion battery electrolytes," *Journal of the Electrochemical Society,* vol. 147, pp. 2874-2879, Aug 2000.

[12] C. S. Johnson, *et al.*, "Anomalous capacity and cycling stability (M= Mn, Ni, Co) in lithium batteries at 50° C," *Electrochemistry Communications,* vol. 9, pp. 787-795, 2007.

[13] Y. Jiang, *et al.*, "Hollow 0.3Li_2MnO_3[middle dot]0.7LiNi0.5Mn0.5O_2 microspheres as a high-performance cathode material for lithium-ion batteries," *Physical Chemistry Chemical Physics,* vol. 15, pp. 2954-2960, 2013.

[14] X. He, *et al.,* "Enhanced electrochemical performance in lithium ion batteries of a hollow spherical lithium-rich cathode material synthesized by a molten salt method," *Nano Research*, vol. 7, pp. 110-118, 2014.

[15] J. B. Fei, *et al.,* "Controlled preparation of MnO_2 hierarchical hollow nanostructures and their application in water treatment," *Advanced Materials*, vol. 20, pp. 452-456, 2008.

[16] B. J. Landi, *et al.*, "Carbon nanotubes for lithium ion batteries," *Energy & Environmental Science*, vol. 2, pp. 638-654, 2009.

[17] K.R. Crompton and B.J. Landi, "Opportunities for Near Zero Volt Storage of Lithium Ion Batteries," *Energy & Environmental Science*, vol. 9, pp. 2219-2239, 2016.

[18] K.R. Crompton, *et al.,* "Lithium rich cathode/graphite anode combination for lithium ion cells with high tolerance to near zero volt storage," *Journal of Power Sources*, vol. 343, pp. 109-118, 2017.

LIST OF ACRONYMS, ABBREVIATIONS, AND SYMBOLS

Acronym/ Abbreviation	Description
AFRL	Air Force Research Laboratory
Al_2O_3	Aluminum Oxide
ALD	Atomic layer Deposition
$AlPO_4$	Aluminium phosphate
BMS	Battery Management System
C-rate	Charge rate
CC	Constant Current
CID	Curent Interrupt Device
CNT	Carbon Nanotube
Cu	Copper
DI H_2O	Distilled water
DOD	Depth Of Discharge
EAP	Electrode Asymptotic Potential
EC	Ethylene Carbonate
EMC	Ethyl Methyl Carbonate
EODV	End Of Discharge Voltage
EV	electric vehicle
Ge	Germanium
GEO	Geostationary orbit
GPS	Global Positioning System
HCl	Hydrogen chloride
He	Helium
HE5050	$0.49Li_2MnO_3 \cdot 0.51LiNi_{0.37}Co_{0.24}Mn_{0.39}O_2$
IR	Infrared
$KMnO_4$	Potassium manganate(VII)
LEO	Low Earth Orbit
Li	Lithium
$LiCoO_2$	Lithium cobalt oxide
$LiPF_6$	Lithium hexafluorophosphate
LPCVD	Low Pressure Chemical Vapor Deposition
MCMB	MesoCarbon MicroBead
MEO/HEO	Medium Earth/High Earth Orbit
$MnCO_3$	Manganese(II) carbonate
MnO_2	Manganese dioxide
$MnSO_4$	Manganese(II) sulfate monohydrate

MWCNT	Multiwall Carbon Nanotubes
NCA	Lithium nickel cobalt aluminum oxide
NH_4CO_3	Ammonium carbonate
Ni-H	Nickel-hydrogen
NiCd	Nickel–cadmium
NMP	N-methyl-1-Purrolidone
NPRL	NanoPower Research Lab
NZVSCE	Near Zero Volt Storage Coulombic Efficiency
O_2	Oxygen
OCV	Open circuit voltage
PECVD	Plasma-enhanced Chemical Vapor Deposition
PTC	Positive Interrupt Coefficient
PVDF	Polyvinylidene Fluoride
R	Resistance
RIT	Rochester Institute of Technology
RLE	Reversible Lithium Excess
SEI	Solid Electrolyte Interface
SEM	Scanning Electron Microscopy
SFG-6	Synthetic flake graphite from TIMREX
Si	Silicon
SLMP	Stabilized Lithium Metal Powder
SOA	State-of-the-art
TGA	Thermogravimetric Analysis
TMA	Trimethylaluminum
UHP Ar	Ultra-high purity argon
V	Voltage
XRD	X-ray Diffraction

DISTRIBUTION LIST

DTIC/OCP
8725 John J. Kingman Rd, Suite 0944
Ft Belvoir, VA 22060-6218 1 cy

AFRL/RVIL
Kirtland AFB, NM 87117-5776 1 cy

Official Record Copy
AFRL/RVSV/Jessica Buckner 1 cy